Ann. Rev. Fluid Mech. 1987. 19 : __-__

DYNAMICS OF TORNADIC THUNDERSTORMS

Joseph B. Klemp

National Center for Atmospheric Research, Boulder, Colorado 80307

1. INTRODUCTION

Tornadic thunderstorms are the most intense and most damaging type of convective storm. Whereas ordinary convective cells grow, produce rain, and then decay over a period of 40 min to an hour, certain thunderstorms may develop a nearly steady-state structure that persists for several hours, producing heavy rain, large hail, damaging surface winds and tornadoes. Although tornadoes may arise in a variety of storm conditions, these long-lived storms produce tornadoes most frequently and generate virtually all of the most damaging ones. Prominent features of these tornadic thunderstorms, which are particularly common in the Great Plains and midwestern regions of the United States, are illustrated in an idealized schematic in Figure 1.

Our understanding of tornadic storms has evolved gradually over the years as technological advances have been made in observing systems and computer models. The first indications that certain storms exhibit a special behavior came from early studies of data from upper-air soundings and surface stations. While most thunderstorms moved with the mean winds over the lower and middle troposphere (Byers & Braham 1949), certain large storms were found to propagate consistently to the right of the mean winds (Byers 1942, Newton & Katz 1958). Observing the shift in the wind direction as storms passed by surface stations, Byers (1942) and later Brooks (1949) surmised that these intense storms have a *cyclonic* circulation (counterclockwise rotation about a vertical axis, viewed from above). Using data from scanning radar and ground observations, case studies of a severe thunderstorm near Wokingham, England (Browning and Ludlam 1962), and another near Geary, Oklahoma (Browning & Donaldson 1963), revealed numerous distinctive features that were strikingly similar in the two storms. Browning & Donaldson proposed that "these two storms may be representative of an important class of local storms; namely those de-

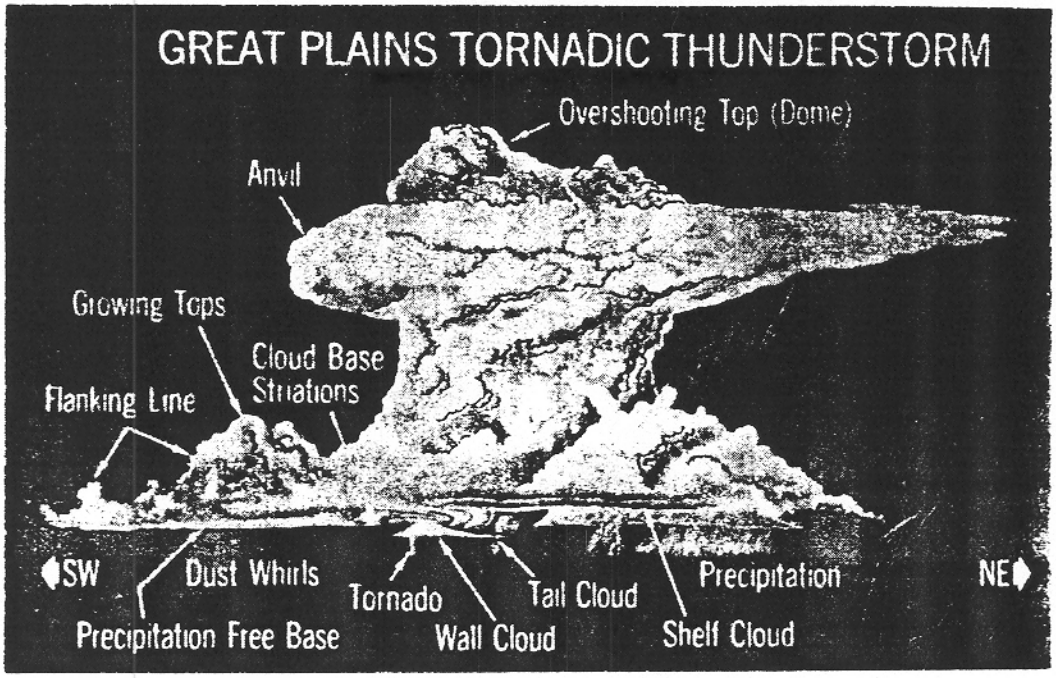

Figure 1 An idealized tornadic thunderstorm as viewed from the southeast. The vertical scale is exaggerated by about a factor of two. (From Joe Golden, NWS–NOAA, personal communication.)

veloping within a strongly sheared environment which remain persistently intense and tend toward a steady state circulation."

Browning (1964) presented a conceptual model to explain the structure of these severe right-moving storms, which he named *supercells*. These storms develop when there is strong vertical shear of the environmental wind, as illustrated in Figure 2*a*, which plots the west-east (U) component of the wind field on the x-axis versus the south-north (V) component on the y-axis. Here, low-level winds (L) from the south turn gradually with height, becoming westerly at higher levels (H) in the upper troposphere; the supercell storm moves to the right of the mean winds, in an easterly direction. Notice that in a coordinate framework moving with the storm, low-level air approaches the storm from the southeast, midlevel air from the south, and upper-level air from the west. Browning's airflow model, shown schematically in Figure 2*b*, depicts a three-dimensional, nearly steady-state circulation (relative to the storm motion) in which warm, moist low-level air feeds continuously into a single large updraft, which is driven by buoyancy derived from the latent heating of condensing water vapor. Evaporative cooling within the region of heaviest precipitation just north of the updraft drives the main downdraft, which ingests air passing around in front of the eastward-moving storm. As the colder and drier downdraft air spreads out beneath the storm, it collides with the warm moist inflow along a line called the *gust front*; this convergence pro-

motes the lifting of potentially buoyant air into the updraft and sustains the convection.

The important feature of this storm structure is the physical separation of the updraft and downdraft circulations such that each branch supports, rather than disrupts, the other. In weakly sheared environments, precipitation forms within the updraft and produces negative buoyancy that destroys the convection. Subsequent research has largely substantiated the basic features of Browning's model.

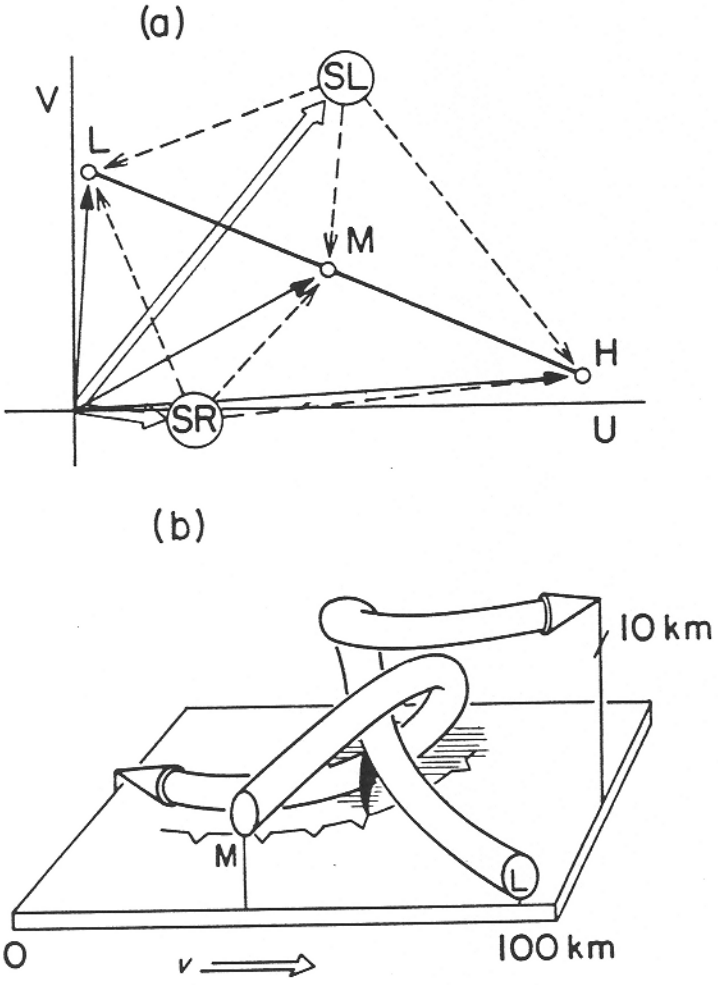

Figure 2 Browning's conceptual model for a right-moving supercell thunderstorm (SR). (*a*) Wind plot illustrating low-(L), middle-(M), and high-(H) level winds relative to the ground (solid arrows) and relative to the storm (dashed arrows). Motion of the SR storm is shown with an open arrow. The motion and relative wind vectors for a possible left-moving supercell (SL) are also shown. (*b*) Three-dimensional airflow within the SR storm, viewed from the south-southeast. Updraft and downdraft circulations are shown relative to the storm motion, depicted with a five-fold exaggeration in the vertical scale. Also depicted are the approximate extent of precipitation at the ground (hatched area), and positions of the gust front (barbed line) and tornado (when present). (Adapted from Browning 1964.)

Occasionally, severe storms are observed that move faster than, and to the left of, the mean winds (*cf.* Hitschfeld 1960, Newton & Fankhauser 1964, Hammond 1967). Browning (1968) noted that the environmental winds shown in Figure 2*a* could also promote a left-moving severe storm (SL). This SL storm experiences relative winds that are a mirror image of the winds in the SR storm about the line LMH. Thus, Browning speculated that the SL storm would similarly have a structure in mirror image to the SR storm shown in Figure 2*b* and that a single thunderstorm might split into two parts, one an SR storm and the other an SL storm, which would move along diverging paths. Hammond (1967) and later others have confirmed this type of SL storm structure, while numerous investigators have documented the splitting and subsequent divergence of severe storms (*cf.* Hitschfeld 1960, Fujita & Grandoso 1968, Achtemeier 1969, Charba & Sasaki 1971, Fankhauser 1971).

By the mid-1970's, technological advances in radar and computers made it possible to investigate the internal structure of supercell thunderstorms in far greater detail. Scanning storms simultaneously with two Doppler radars permitted calculation of the three-dimensional wind field within storms (Ray *et al.* 1975, Miller 1975), while three-dimensional numerical models began to simulate storms in highly idealized environments (Wilhelmson 1974, Miller & Pearce 1974, Schlesinger 1975). More recently, simulations of specific supercell thunderstorms have reproduced many of the important features of the observed storms (Klemp *et al.* 1981, Wilhelmson & Klemp 1981). With more comprehensive data, new theories arose to explain the mechanisms that govern the important physical processes in these severe thunderstorms, such as the development of rotation, storm splitting, storm propagation, the preferential enhancement of right-moving cyclonically rotating storms, and the intensification of low-level rotation as a storm enters its tornadic phase.

In the following sections, I discuss the essential fluid processes promoting these special storm features that characterize the tornadic supercell thunderstorm. In doing so, I draw heavily from the results of three-dimensional numerical-modeling studies, in which storms can be generated under controlled conditions and which provide complete kinematic and thermodynamic data both in and around a storm. However, although these models have demonstrated good qualitative agreement with observed storms, some of the mechanisms derived from the detailed analyses of simulated storms must still be tested against future data that will be obtained from increasingly sophisticated storm-observing systems.

Over the past several years, a number of excellent reviews have comprehensively documented the progress in convective-storm research (*cf.* Lilly 1979, Houze & Hobbs 1982, Kessler 1985). In this more limited review, I focus on selected aspects of tornadic thunderstorm dynamics, without

attempting to represent all points of view, in order to avoid undue distraction for the reader unfamiliar with this topic.

2. EARLY DEVELOPMENT OF ROTATION

During its early development, an isolated cumulus grows as a buoyant thermal (or perhaps as a cluster of thermals). At this stage, it has long been known (Byers & Braham 1949) that wind shear inhibits the convection, tending to tear apart the rising thermals. However, when a vigorous updraft does develop in a sheared environment, it invariably exhibits significant rotation about a vertical axis, typically in the form of a pair of counterrotating vortices (Wilhelmson 1974, Schlesinger 1975, Kropfli & Miller 1976, Wilhelmson & Klemp 1978). This vortex-pair circulation arises as a result of the tilting into the vertical of horizontal vortex lines embedded initially in the environmental shear. Rotunno (1981) pointed out that the manner in which tilting produces vertical vorticity in the early convection may differ significantly from that in the mature thunderstorm propagating transverse to the mean winds.

To illustrate the evolution of rotation, we consider the basic governing equations that describe the relevant storm processes. For a compressible atmosphere, the appropriate analogue to the incompressible Boussinesq equations may be written in the following form (Ogura & Phillips 1962, Lilly 1979):

$$\frac{\partial \boldsymbol{v}}{\partial t} + \boldsymbol{v} \cdot \nabla \boldsymbol{v} + \nabla \pi = B\hat{\boldsymbol{k}} + \boldsymbol{F} \tag{1}$$

$$\nabla \cdot \bar{\rho} \boldsymbol{v} = 0, \tag{2}$$

where $\boldsymbol{v} = (u, v, w)$ is the three-dimensional velocity vector in Cartesian coordinates (x, y, z), $\boldsymbol{F}$ represents the turbulent mixing, $\hat{\boldsymbol{k}}$ is the unit vector in the vertical direction, and B is the total perturbation buoyancy, including the influences of temperature and water vapor as well as drag caused by liquid water. Here, $\pi = p'/\bar{\rho}$, where p' is the pressure perturbation about a mean state corresponding to an adiabatic atmosphere (i.e. the mean pressure $\bar{p}$ and mean density $\bar{\rho}$ are related by $\bar{p} \sim \bar{\rho}^{c_p/c_v}$), and henceforth we refer to π as the pressure. The Coriolis force has been omitted from (1), since it does not play a fundamental role in the storm dynamics to be discussed (Klemp & Wilhelmson 1978).

Taking the curl of (1) then yields expressions for the vertical (ζ) and horizontal (ω_h) components of vorticity $\boldsymbol{\omega} = \nabla \times \boldsymbol{v}$:

$$\frac{d\zeta}{dt} = \underbrace{\boldsymbol{\omega}_h \cdot \nabla_h w}_{\text{tilting}} + \underbrace{\zeta \frac{\partial w}{\partial z}}_{\text{stretching}} + \underbrace{F'_\zeta}_{\text{mixing}}, \tag{3}$$

$$\frac{d\omega_h}{dt} = \underbrace{\boldsymbol{\omega}\cdot\boldsymbol{\nabla}\boldsymbol{v}_h}_{\substack{\text{tilting and}\\ \text{stretching}}} + \underbrace{\boldsymbol{\nabla}\times(B\hat{\boldsymbol{k}})}_{\substack{\text{baroclinic}\\ \text{generation}}} + \underbrace{\boldsymbol{F}_h'}_{\text{mixing}}, \tag{4}$$

where $\boldsymbol{v}_h = (u, v)$ and F_ζ', $\boldsymbol{F}_h'$ are the respective mixing terms with $\boldsymbol{F}' = \boldsymbol{\nabla}\times\boldsymbol{F}$, and d/dt is the Lagrangian time derivative.

Focusing on the generation of vertical vorticity, we see that the first term on the right-hand side of (3) contributes to ζ by tilting horizontal vortex lines into the vertical, while the second term alters ζ through the vertical stretching of vortex tubes. Clearly, if convection begins in an environment containing no vertical vorticity, then the initial production of ζ must arise through the tilting of horizontal vorticity contained in the ambient wind shear. The important parameter characterizing the vertical wind shear is the environmental wind-shear vector $\boldsymbol{S} = d\boldsymbol{V}/dz$, where $\boldsymbol{V} = (U, V)$. $\boldsymbol{S}$ has two components: speed shear represented by $|\boldsymbol{S}|$, and directional shear caused by turning of the shear vector. Notice that the wind field shown in Figure 2*a* has only speed shear, with $\boldsymbol{S}$ being oriented parallel to the line LMH. Numerical storm simulations have shown that a unidirectional wind shear is sufficient to produce supercell-like storms with characteristic structure similar to that shown in Figure 2*b* (Klemp & Wilhelmson 1978). However, directional shear also exerts important influences on storm evolution, as is discussed in Section 4.

For simplicity, consider first an isolated cumulus growing in unidirectional wind shear in which the westerly velocity U increases with height and V=0. In its early convective growth, the cloud moves roughly with the mean westerly flow (averaged over the depth of the cloud). Thus, in a storm-relative framework, low-level inflow approaches the cloud from the east while upper-level outflow returns toward the east, as illustrated in Figure 3*a*. A vortex-pair circulation develops as south-north-oriented vortex lines are swept into the updraft and tilted into the vertical.

This mechanism is contained in the linearized vertical vorticity equation given by (ignoring the mixing term)

$$\frac{d\zeta}{dt} = \frac{dU}{dz}\frac{\partial w}{\partial y}. \tag{5}$$

Positive (cyclonic) vertical vorticity is generated along the southern flank of the updraft ($\partial w/\partial y > 0$), while negative (anticyclonic) vorticity is produced on the northern flank ($\partial w/\partial y < 0$). As the updraft intensifies, vorticity that has been tilted into the vertical can be amplified substantially by the stretching of vortex tubes, which is a nonlinear effect.

3. STORM SPLITTING

Although the cloud in Figure 3*a* is still a rather ordinary cumulus, forcing influences are already promoting its transition to a supercell storm. As

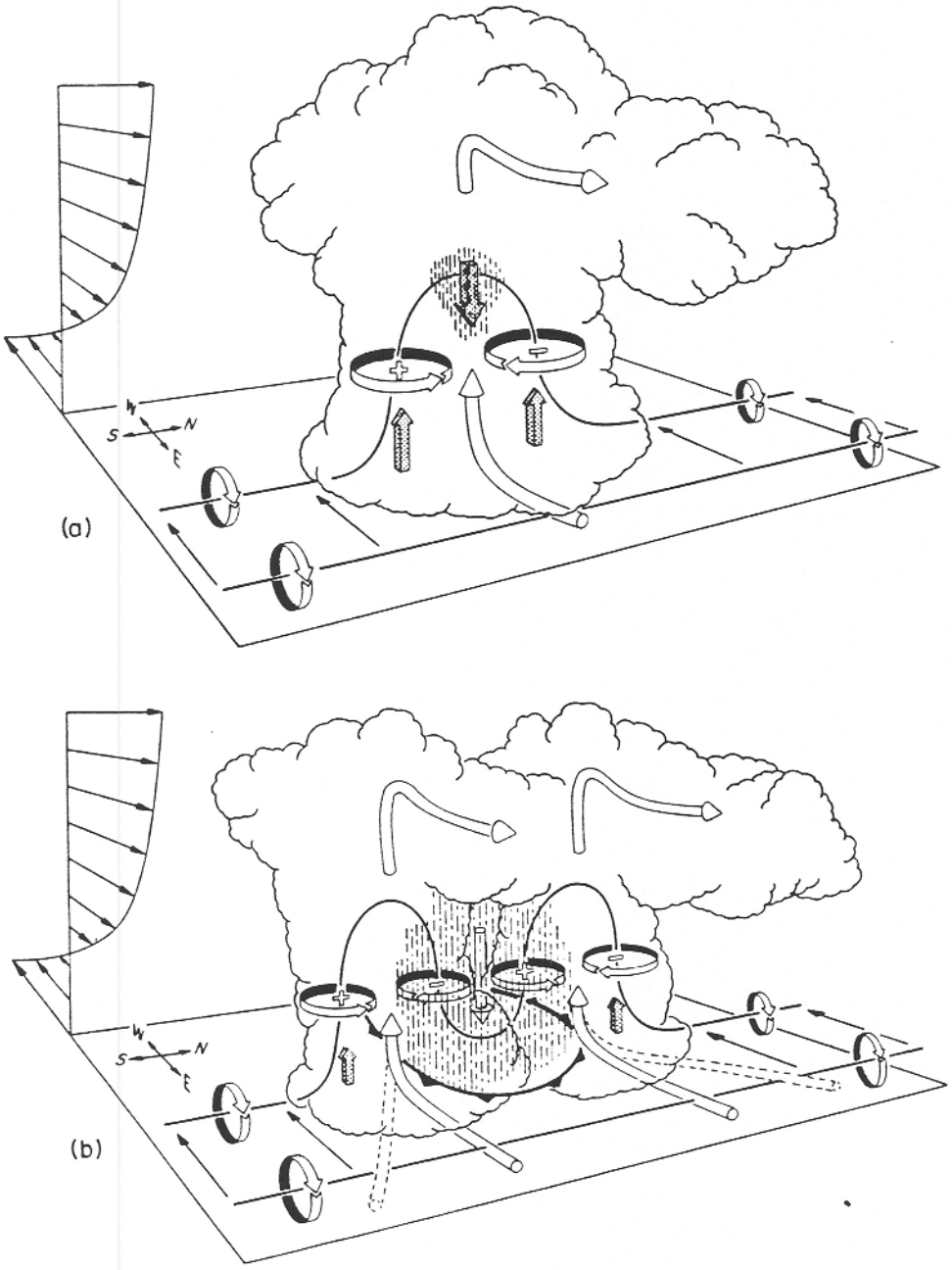

Figure 3 Schematic depicting how a typical vortex tube contained within (westerly) environmental shear is deformed as it interacts with a convective cell (viewed from the southeast). Cylindrical arrows show the direction of cloud-relative airflow, and heavy solid lines represent vortex lines with the sense of rotation indicated by circular arrows. Shaded arrows represent the forcing influences that promote new updraft and downdraft growth. Vertical dashed lines denote regions of precipitation. (*a*) Initial stage: Vortex tube loops into the vertical as it is swept into the updraft. (*b*) Splitting stage: Downdraft forming between the splitting updraft cells tilts vortex tubes downward, producing two vortex pairs. The barbed line at the surface marks the boundary of the cold air spreading out beneath the storm. (Adapted from Rotunno 1981.)

precipitation accumulates within the updraft, increasing negative buoyancy produces a downdraft within the cloud. Enhanced by evaporative cooling, the downdraft outflow at the surface, being colder than the surrounding environment, spreads out beneath the storm. In weak wind shear, this outflow spreads out in all directions, cutting off the supply of warm moist air, and the storm cell dissipates rapidly. However, in strong shear (i.e. $|\boldsymbol{S}| \simeq 10^{-2}$ s^{-1}, or 10 m s^{-1} per km over the lowest several km), two factors act to extend the longevity of the storm: storm-relative low-level inflow from the east prevents the cold air from moving out ahead of the storm (Wilhelmson & Klemp 1978, Thorpe & Miller 1978), and lifting pressure gradients reinforce new updraft growth on the southern and northern flanks of the central updraft (Schlesinger 1980, Rotunno & Klemp 1982). In response to these forcing influences, the updraft splits gradually into two cells that move laterally apart, as illustrated in Figure 3*b*.

The lifting vertical pressure gradients appear to be the fundamentally important factor in splitting the cloud into two cells that then move apart. Although the cold low-level downdraft outflow increases the convergence along the updraft flanks, numerical simulations demonstrate that updraft splitting occurs even if this central downdraft is prevented from forming (Rotunno & Klemp 1982, 1985). This is accomplished in the models by not allowing any precipitation to fall relative to the surrounding air. Without this falling precipitation, the negative buoyancy required to generate the downdraft is greatly reduced.

The origin of these lifting forces can be elucidated through a detailed analysis of the terms in the vertical momentum equation, as generated by three-dimensional storm-simulation models. By dividing the pressure into components $\pi = \pi_{dn} + \pi_b$, produced by dynamic interactions π_{dn} and through buoyancy effects π_b, the vertical component of (1) can be written in the form

$$\frac{\partial w}{\partial t} = - \underbrace{\boldsymbol{v}\cdot\boldsymbol{\nabla} w}_{\text{advection}} - \underbrace{\frac{\partial \pi_{dn}}{\partial z}}_{\substack{\text{dynamics}\\ \text{forcing}}} \underbrace{- \left(\frac{\partial \pi_b}{\partial z} - B\right)}_{\substack{\text{buoyancy}\\ \text{forcing}}} + \underbrace{F_w}_{\text{mixing}} , \tag{6}$$

and expressions for the dynamics and buoyancy components of the pressure are obtained from the divergence of (1):

$$\boldsymbol{\nabla}\cdot(\bar{\rho}\boldsymbol{\nabla}\pi_{dn}) = -\boldsymbol{\nabla}\cdot(\bar{\rho}\boldsymbol{v}\cdot\boldsymbol{\nabla}\boldsymbol{v}) + \boldsymbol{\nabla}\cdot\bar{\rho}\boldsymbol{F} \tag{7}$$

$$\boldsymbol{\nabla}\cdot(\bar{\rho}\boldsymbol{\nabla}\pi_b) = \frac{\partial}{\partial z}(\bar{\rho}B). \tag{8}$$

The dynamics forcing term in (6) thus represents the contribution to vertical accelerations from the portion of the vertical pressure gradient created

by dynamic interactions, while the buoyancy forcing term includes the pressure gradient arising through buoyancy effects. Since a large portion of the buoyancy pressure gradient may be balanced by the buoyancy term itself, the buoyancy forcing, as defined in (6), represents the net influence of buoyancy on vertical accelerations. The divergence of the turbulent mixing term $\nabla \cdot \bar{\rho}\boldsymbol{F}$ has a generally minor influence on the pressure, since these terms largely cancel through the continuity equation (2); thus, they are omitted in further discussions (Klemp & Rotunno 1983). Pressure decompositions similar to this have been used to analyze numerous aspects of storms simulated with three-dimensional models (Wilhelmson 1974, Schlesinger 1980, Rotunno & Klemp 1982, 1985, Klemp & Rotunno 1983).

Schlesinger (1980) first noted that the lifting pressure gradients on the flanks of a splitting updraft are dynamic in origin. Rotunno & Klemp (1982) proposed that these lifting pressure gradients on the updraft flanks are induced by the midlevel rotation. To assess the influence of rotation on the pressure, we expand the right-hand side of (7) in the form

$$\nabla \cdot (\bar{\rho}\nabla\pi_{dn}) = -\bar{\rho}\underbrace{\left[\left(\frac{\partial u}{\partial x}\right)^2 + \left(\frac{\partial v}{\partial y}\right)^2 + \left(\frac{\partial w}{\partial z}\right)^2 - \frac{d^2 ln\bar{\rho}}{dz^2}w^2\right]}_{\text{fluid extension terms}}$$

$$- 2\bar{\rho}\underbrace{\left[\frac{\partial v}{\partial x}\frac{\partial u}{\partial y} + \frac{\partial u}{\partial z}\frac{\partial w}{\partial x} + \frac{\partial v}{\partial z}\frac{\partial w}{\partial y}\right]}_{\text{fluid shear terms}}. \tag{9}$$

Consider first the fluid shear term $\partial v/\partial x \cdot \partial u/\partial y$. For a wind field in pure rotation, this term is simply $-\frac{1}{4}\zeta^2$. For purposes of qualitative analysis, note that in the interior of a flow, the Laplacian of a variable is roughly proportional to the negative of the variable itself (i.e. $\nabla^2\pi \sim -\pi$). Combining these relations then yields

$$\pi_{dn} \sim -\zeta^2, \tag{10}$$

which suggests that the strong midlevel rotation on the updraft flank (see Figure 3*b*) acts to lower the pressure, and thereby induces updraft growth on these flanks. The second and third fluid shear terms in (9) are related similarly to the x- and y- components of vorticity, respectively. These terms are amplified by the vortex ring that forms around the updraft because of the horizontal buoyancy gradients on its flanks [i.e. through the baroclinic generation term in Equation (4)]. Therefore, these two rotational terms also contribute to lowering the pressure on the flanks of the midlevel updraft, although (unlike the first term) they are not specific to the flanks that are transverse to the shear. Rotunno & Klemp (1982) found that the fluid extension terms in (9) do not contribute to the lifting pressure gradients on the updraft flanks. Consequently, strong rotation

about the vertical axis appears to be the special feature that promotes the splitting within evolving supercell thunderstorms.

As the splitting progresses and the two updraft centers move apart laterally, the downdraft dividing the two cells tilts the vortex lines downward, producing two vortex-pair circulations as shown in Figure 3*b* (Rotunno 1981). As each updraft begins to propagate transverse to the mean wind shear, the direction of storm-relative inflow turns as indicated by the dashed cylindrical arrows in Figure 3*b*. In this configuration, the low-level inflow contains a streamwise component of the horizontal shear vorticity, as well as the transverse component that produced the original vortex pair. Browning & Landry (1963) and Barnes (1970) proposed that the tilting of the streamwise vorticity in the environmental shear was the important contributor to the rotation in supercell storms. Rotunno (1981), Lilly (1982), and Davies-Jones (1984) also emphasized the importance of the streamwise vorticity; using simplified linear models, they demonstrated that if the environmental shear vector is parallel to the storm-relative inflow, the vertical vorticity generated through tilting will tend to be in phase with the vertical velocity (as opposed to the transverse component that produces vertical vorticity maxima on the updraft flanks, as shown in Figure 3*a*).

Following Lilly (1986a), we consider a steady updraft propagating transverse to the environmental wind shear (i.e. to the south at velocity c_y in the situation shown in Figure 3). In a coordinate framework relative to the moving updraft, flow approaches from the south with a velocity $-c_y$. The linear vertical vorticity equation (3) then becomes (ignoring mixing)

$$-c_y \frac{\partial \zeta}{\partial y} = \frac{dU}{dz}\frac{\partial w}{\partial y}, \tag{11}$$

which can be integrated immediately, with the result being

$$\zeta = \frac{dU}{dz}\frac{w}{(-c_y)}. \tag{12}$$

Thus, the vertical vorticity is coincident with the vertical velocity in this simplified situation.

Davies-Jones (1984) and Rotunno & Klemp (1985) extended the linear theory by providing interpretations of vertical vorticity generation within storms that remain valid even in fully nonlinear flow. Using the equations of motion as written in (1) and (2), we can show through Ertel's theorem (see Dutton 1976, p. 382) that for a conserved scalar variable Θ depending only on the thermodynamic properties of the flow it follows that

$$\frac{d}{dt}\left\{\frac{\boldsymbol{\omega}\cdot\boldsymbol{\nabla}\Theta}{\bar{\rho}}\right\} = 0. \tag{13}$$

Here, we identify Θ as the entropy of the moist fluid flow. Since $\boldsymbol{\omega}\cdot\boldsymbol{\nabla}\Theta = 0$ in the initial, undisturbed state, it will remain zero throughout

the evolving storm. This result means that vortex lines must lie along isentropic surfaces. Thus, as isentropic surfaces are drawn up into the storm, their embedded vortex lines are similarly deformed.

This effect was illustrated by Rotunno & Klemp (1985) within a numerically simulated storm evolving in a unidirectional (west-to-east) shear (see Figure 4). In the initial state, the isentropic surfaces are horizontal

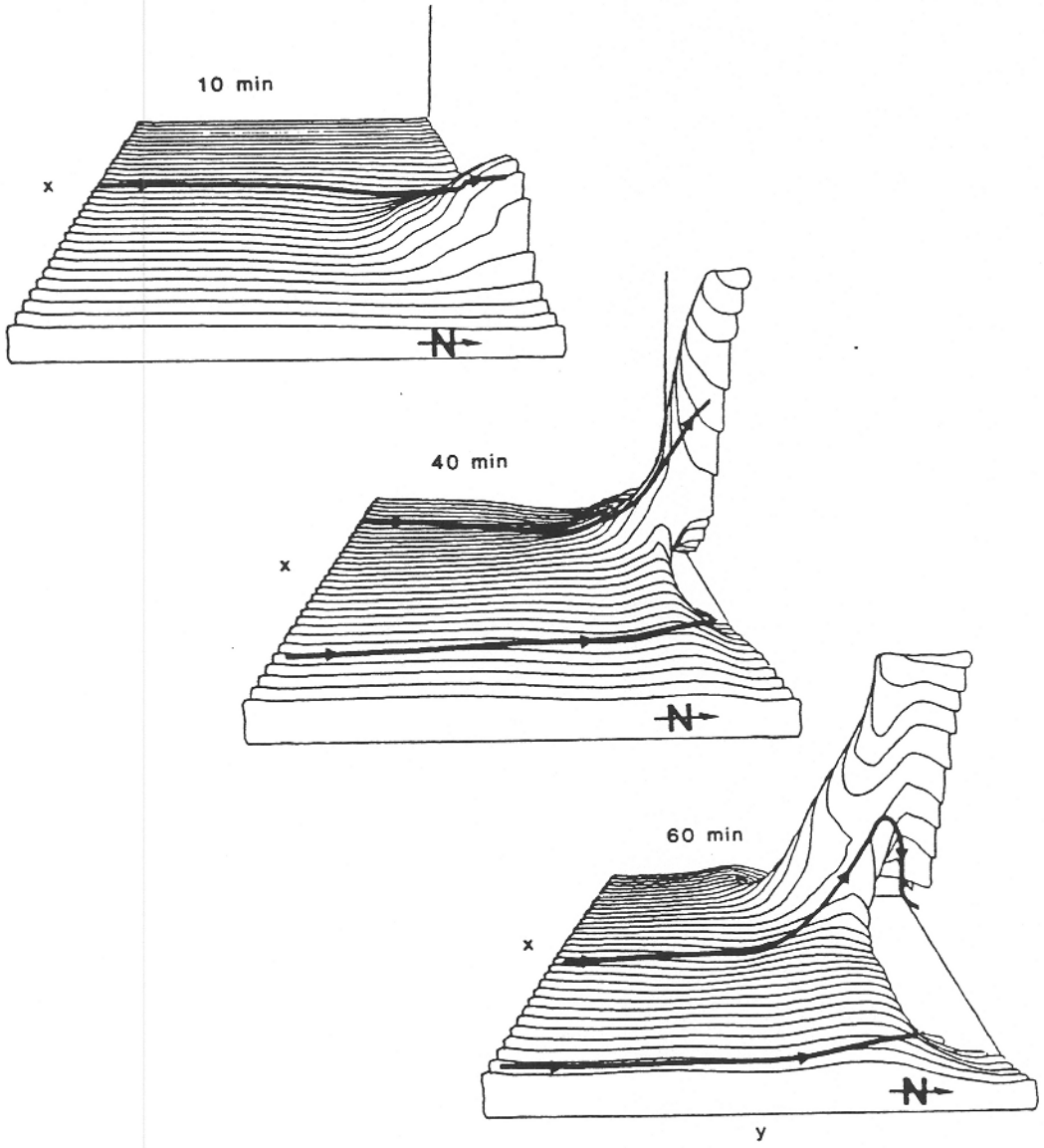

Figure 4 Numerically simulated three-dimensional perspective (viewed from the east) of a low-level isentropic surface that is being drawn up into the storm updraft at t=10, 40, and 60 min. The environmental wind shear is directed from west to east, and the flow is symmetric about the vertical plane along the northern border. Vortex lines (heavy solid lines) lie approximately on the isentropic surface. The base plane spans 20 km in the south-north direction, and the vertical scale is exaggerated by a factor of two. (From Rotunno & Klemp 1985.)

and the vortex lines in the environmental shear are oriented south to north. As low-level flow rises into the updraft (t = 10 min) the vortex lines follow the deforming isentropic surfaces, producing cyclonic vertical vorticity on the southern flank and anticyclonic vorticity along the northern flank (not shown). After the splitting updraft begins moving toward the south (t = 40 min), vortex lines are continuously turned into the vertical along the southern flank as the isentropic surfaces are lifted into the updraft. As the evaporatively cooled downdraft (centered on the symmetry plane) brings midlevel air to the ground, a depression appears in the low-level isentropic surface (t = 40, 60 min). Vortex lines turned upward along the southern updraft flank turn back downward and produce anticyclonic vorticity on the northern flank (t = 60 min). At t = 40 and 60 min, the vortex lines shown in the foreground curl underneath along the boundary of the cold downdraft and disappear from view. This redirection of vortex lines is discussed further in Section 6.

4. PREFERENTIAL ENHANCEMENT OF CYCLONICALLY ROTATING STORMS

The splitting process described above leads naturally to a pair of rotating storms — a cyclonic one moving to the right of the mean winds and an anticyclonic one moving to the left. However, right-moving, cyclonically rotating supercell storms are, in fact, observed far more commonly. Davies-Jones (1985) notes that out of 143 storms in which radar detected strong rotation, only 3 rotated anticyclonically. Although it is tempting to attribute this bias to the ambient rotation in the atmosphere caused by the Coriolis force (which is cyclonic in the Northern Hemisphere), scale analyses suggest that this effect should be small (Morton 1966). Numerical storm simulations indicate that the Coriolis force does enhance the cyclonic rotation in the right-moving storm but does not selectively suppress the anticyclonically rotating storm (Klemp & Wilhelmson, 1978).

By simulating supercell storms in a variety of wind-shear conditions, Klemp & Wilhelmson (1978) demonstrated that a clockwise turning with height of the environmental wind-shear vector is the key factor that selectively promotes the cyclonic, right-moving storm. This turning is apparent in the composite wind sounding (Figure 5) compiled by Maddox (1976) for a large number of tornadic storms. Notice that if we superimpose x, y-axes over the U, V-axes in Figure 5, the wind-shear vector $\boldsymbol{S}$ is locally tangent to the curve $V(U)$ at all levels in the sounding. In this composite, the wind-shear vector turns clockwise with height, from the north-northeast near the surface to the east-southeast at 700 mbar (about 3 km above the ground).

Figure 6 illustrates the evolving storm structures for two wind profiles — one having a unidirectional environmental wind shear vector (top) and the other having a shear vector that turns clockwise with height through

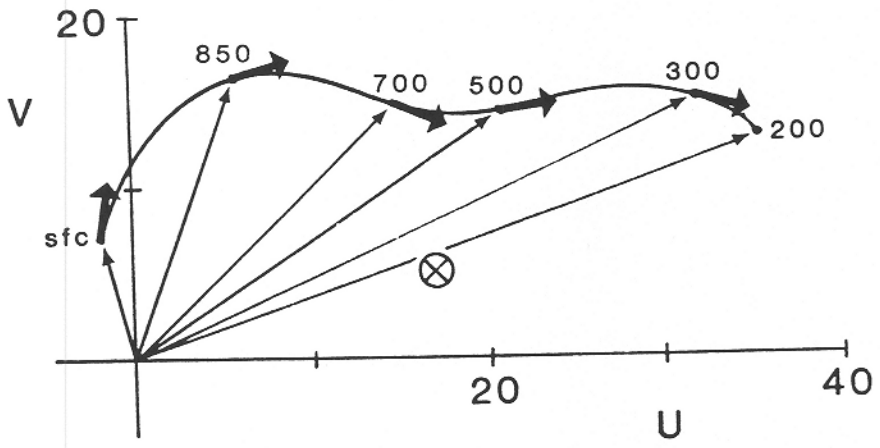

Figure 5 Mean wind sounding (in m s^{-1}) for 62 tornado outbreak cases. The soundings are composited by computing the winds at each level relative to the estimated storm motion. Heavy arrows indicate the direction of the shear vector at each level (labeled in mbar). The estimated mean storm motion is denoted by ⊗. (Adapted from Maddox 1976.)

the lower levels (bottom). With the winds below 2.5 km given by the dashed line in the accompanying wind plot, the initial cloud splits into two storms after 40 min that move apart as they propagate to the northeast. In the absense of surface drag and Coriolis effects, they evolve into identical, mirror-image right- and left-moving storms. In this simulation the line of symmetry is oriented east–west and moves toward the north at 12.7 m s^{-1}. When the low-level shear vector turns cyclonically with height, the initial convective cell evolves into an intense, cyclonically rotating right-moving storm, while on the left flank, only weaker, short-lived cells form along the gust front. Notice that the significant factor here is the turning of the wind-shear vector, *not* the turning of the wind vector itself. (In either wind profile, the ground-relative winds turn clockwise with height.)

Rotunno & Klemp (1982) found that the basis for the selective enhancement of either the right- or left-moving storm is contained within linear theory. As an initially axisymmetric updraft interacts with a mean wind shear $\boldsymbol{S}$ that turns clockwise with height, favorable vertical pressure gradients are dynamically induced on the right flank while unfavorable gradients arise on the left. To demonstrate this effect, consider an updraft perturbation in a homogeneous fluid ($B = 0$). The linearized inviscid vertical momentum and pressure equations (6)–(8) are then simply

$$\frac{dw}{dt} = -\frac{\partial \pi}{\partial z}, \tag{14}$$

$$\nabla^2 \pi = -2\boldsymbol{S} \cdot \nabla_h w. \tag{15}$$

We can evaluate the qualitative behavior of (15) by again using the approximation $\nabla^2\pi \sim -\pi$, which yields

$$\pi \sim \boldsymbol{S} \cdot \boldsymbol{\nabla}_h w. \tag{16}$$

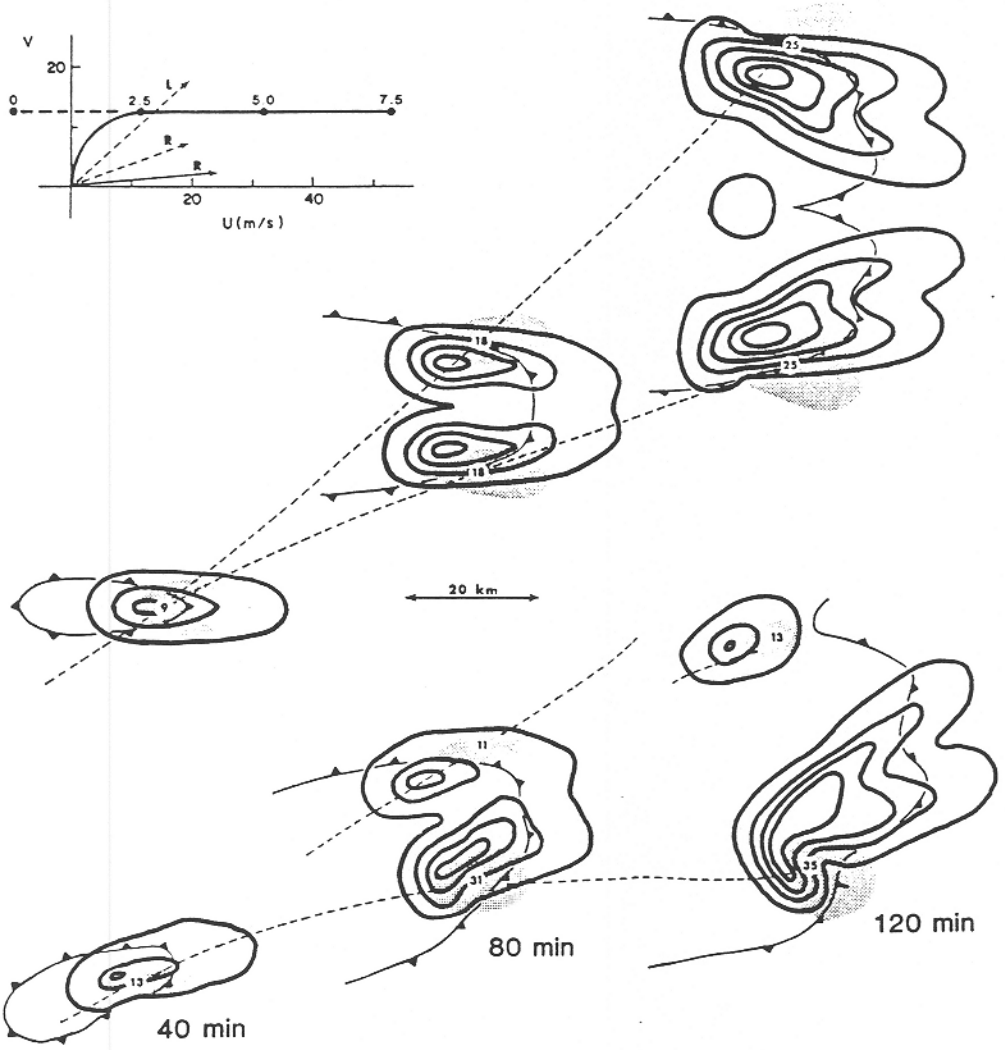

Figure 6 Plan views of numerically simulated thunderstorm structures at 40, 80, and 120 min for two environmental wind profiles (displayed at upper left) having wind shear between the surface and 7.5 km. The storm system in the lower portion of the figure evolves in response to the wind profile in which $\boldsymbol{S}$ turns clockwise with height between the ground and 2.5 km (heavy solid line in wind plot), while the upper system develops when $\boldsymbol{S}$ is unidirectional (same wind profile except following the heavy dashed line below 2.5 km). The plan views depict the low-level (1.8 km) rainwater field (similar to radar reflectivity) contoured at 2 g kg^{-1} intervals, the midlevel (4.6 km) updraft (shaded regions), and the location of the surface cold-air outflow boundary (barbed lines). The maximum updraft velocity is labeled (in m s^{-1}) within each updraft at each time. The dashed lines track the path of each updraft center. Arrows in the wind plot indicate the superceell propagation velocities for the unidirectional (dashed) and turning (solid) wind shear profiles. (Adapted from Klemp & Weisman 1983.)

Thus, linear theory suggests that as an updraft interacts with the shear flow, a high-to-low pressure gradient develops across the updraft in the direction of the local shear vector at each level. For a constant shear magnitude, this pressure effect increases in amplitude with height beneath the level of the maximum updraft velocity.

To visualize the influences of these shear-induced pressure variations, consider first the unidirectional shear profile represented in Figure 3. Here the shear vector points from west to east at all levels, producing high pressure on the upshear (west) side of the updraft and low pressure on the downshear (east) side, as depicted in Figure 7*a*. As the updraft intensity increases above the ground, these pressure perturbations promote low-level lifting on the downshear side (and descent on the upshear side) that reinforces the storm inflow. However, these vertical pressure gradients do not contribute to a preferential growth on either of the flanks that are transverse to the shear or to storm splitting (which, as discussed in Section 3, is an inherently nonlinear effect).

Expressing the linearized vertical vorticity equation (3) in terms of $\boldsymbol{S}$, we have

$$\frac{d\zeta}{dt} = \boldsymbol{k} \cdot (\boldsymbol{S} \times \nabla_h w), \tag{17}$$

which indicates that the vortex pair generated through tilting is oriented at right angles to the shear vector. For the unidirectional shear in Figure 7*a*, Equation (17) is identical to Equation (5), producing cyclonic and anticyclonic vorticity on the southern and northern flanks, respectively.

Figure 7*b* illustrates the corresponding situation when $\boldsymbol{S}$ turns clockwise with height through the lower levels of the atmosphere. Here, the winds change with height from easterly, to southerly, and finally to westerly, such that $\boldsymbol{S}$ turns through 180° (pointing toward the north at the ground, and turning to the east and then to the south at higher levels). In this situation, the turning shear vector produces vertical pressure gradients that favor ascent on the southern flank (designated the right flank by facing in the direction of the mean wind-shear vector) and descent on the northern (left) flank. This influence, in conjunction with the nonlinear processes that promote splitting, enhances the development of the right-moving storm and inhibits the growth of the left-moving storm. When there is significant turning of the shear vector, growth on the left flank may be suppressed to the extent that there would be no apparent splitting at all; the initial storm just begins moving to the right of the mean winds at a certain stage in its development (as occurs in the storm simulation with turning shear in Figure 6). As the vortex pair forms perpendicularly to the shear vector, the production of cyclonic vorticity is also on the right flank, where the favorable pressure gradients are promoting new updraft growth. For a wind profile in which $\boldsymbol{S}$ turns counterclockwise with height,

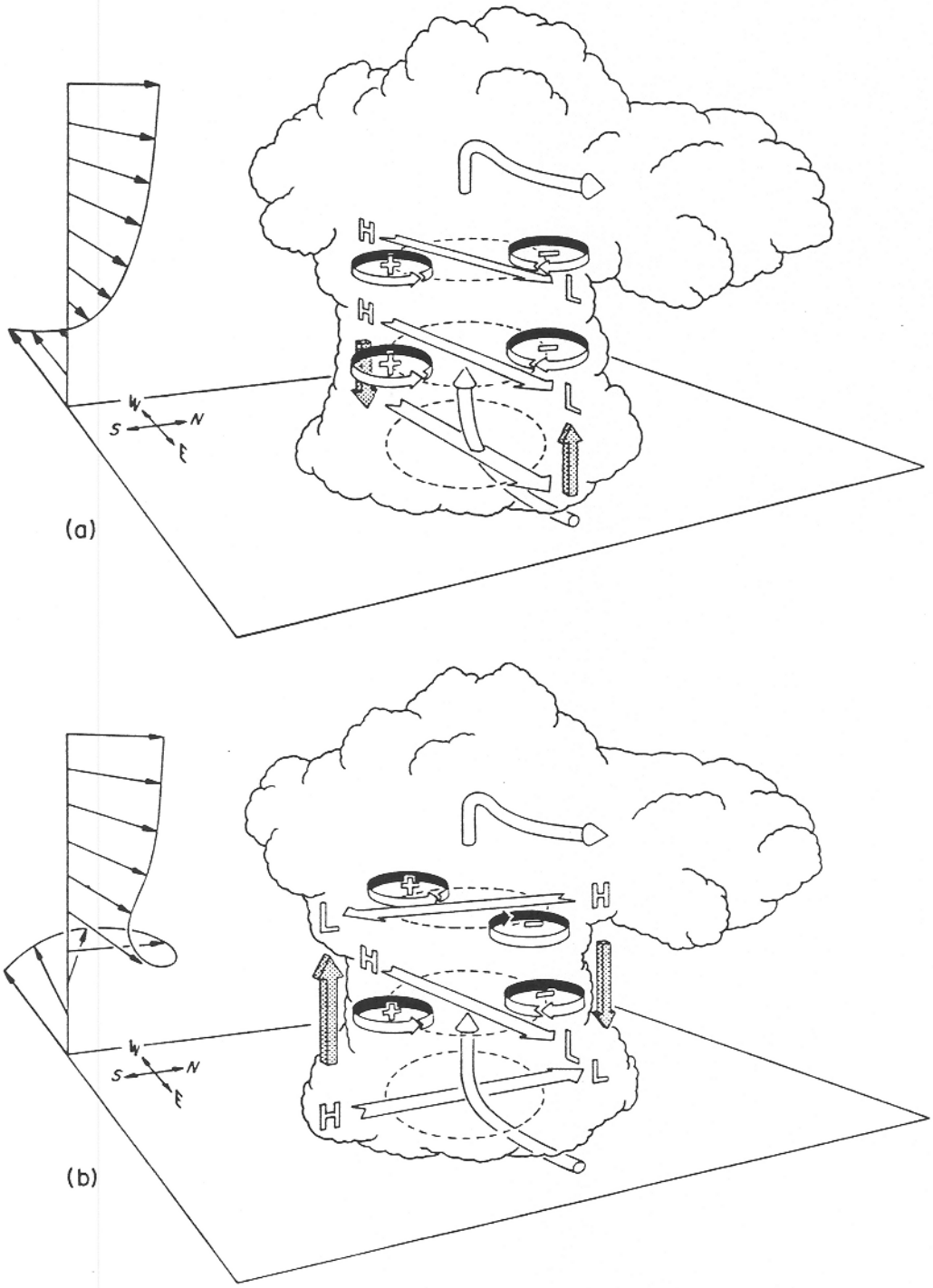

Figure 7 Schematic illustrating the pressure and vertical vorticity perturbations arising as an updraft interacts with an environmental wind shear that (*a*) does not change direction with height and (*b*) turns clockwise with height. The high (H) to low (L) horizontal pressure gradients parallel to the shear vectors (flat arrows) are labeled along with the preferred location of cyclonic (+) and anti-cyclonic (−) vorticity. The shaded arrows depict the orientation of the resulting vertical pressure gradients. (Adapted from Rotunno & Klemp 1982.)

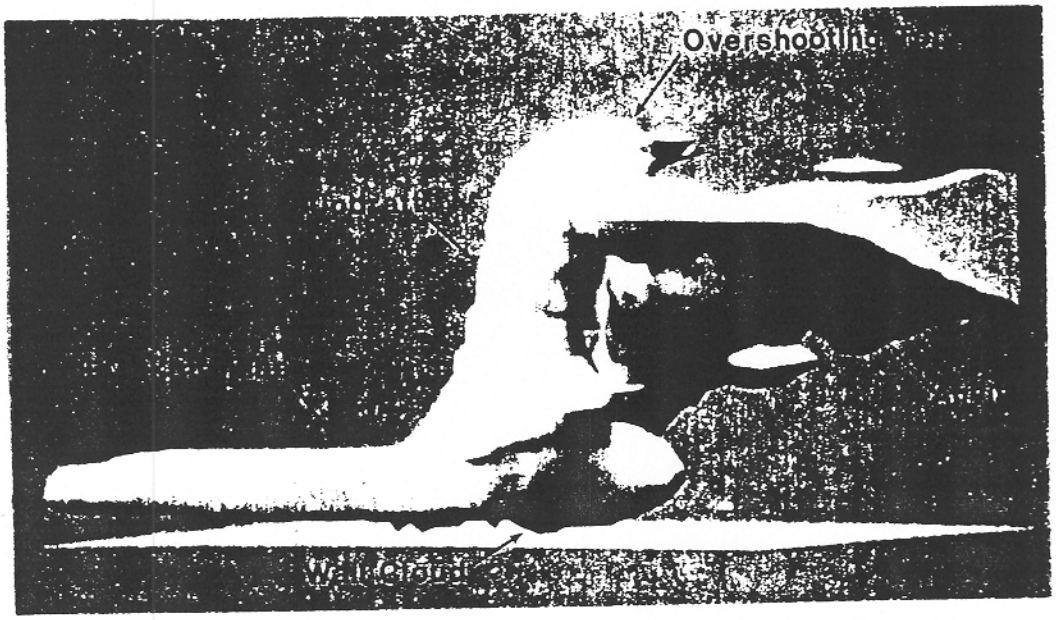

Figure 8 Numerically simulated cloud depicting a supercell storm in its mature phase. The unidirectional environmental wind-shear vector points toward the east (i.e. increasing westerlies with height), and the storm is viewed from the southeast. The shaded surface coincides with the 0.1 g kg^{-1} contour in the model cloud-water field. The storm simulation is described in detail by Rotunno & Klemp (1985).

the situation would be reversed and the left-moving, anticyclonically rotating member of the split pair would be selectively enhanced.

5. STORM PROPAGATION

As storms begin to propagate with a component tranvervse to the mean winds, those that will become supercell thunderstorms generally continue to intensify and evolve toward a mature structure such as that shown schematically in Figure 2*b*. Their ability to persist in a quasi-steady-state configuration for a period of hours is a truly remarkable feature of these storms. Browning & Foote (1976) analyzed the radar observations of a storm in northeastern Colorado that maintained a supercellular structure for more than 5 hours and produced a swath of damaging hail (some as large as baseballs) over a 300-km-long path.

Comprehensive analyses of tornadic thunderstorms using multiple-Doppler radar observations have provided detailed documentation of the important features of these storms (*cf.* Ray *et al.* 1975, 1981; Brandes 1977, 1978; Eagleman & Lin 1977). Numerical simulations have also provided an informative view of supercell thunderstorms, particularly those conducted in idealized environmental conditions, where various environmental influences can be selectively evaluated (*cf.* Weisman & Klemp 1982, 1984). Figure 8 depicts the model-equivalent of the visible cloud for a right-moving supercell storm during its mature phase for a case of

unidirectional wind shear in the absence of Coriolis effects. Even under these idealized conditions, there are strong qualitative similarities with the illustration in Figure 1. In this situation, a mirror-image, left-moving storm also develops, which is accommodated using appropriate symmetry conditions along the northern boundary of the computational domain.

The flow structure within this quasi-steady storm (see Figure 9) exhibits features that are characteristic of supercell storms. At low levels, there is a zone of convergence (gust front) where the warm, moist low-level inflow collides with the cold downdraft outflow. Strong cyclonic rotation is visible within the midlevel (4 km) updraft, and this flow turns downstream into the anvil outflow at higher levels. The hook-like feature on the southern side of the rainwater field at low and midlevels corresponds to the hook echo that is frequently observed by radar in tornadic storms. Although the environmental winds blow only in the east–west direction, this storm is propagating toward the south at about 5 m s^{-1}.

The mechanism that causes the transverse propagation of supercell storms has remained an intriguing although illusive issue over the years. Researchers have proposed a variety of theories that appeal to a diverse spectrum of physical processes. Several of these interesting approaches are summarized below.

Analogies with Obstacle Flow

Even in the early storm observations, researchers recognized that the updrafts in large storms remain erect, in defiance of the strong environmental wind shear in which they are embedded. Substantial portions of environmental air therefore diverge and flow around the storm in a manner that resembles flow past a bluff obstacle at high Reynolds number, with separation occurring behind the obstacle (*cf.* Newton & Newton 1959, Newton 1963, and also the flow at $z = 8$ km in Figure 9). From controlled laboratory experiments it is well known that flow past a cylinder produces high pressure near the forward stagnation point and low pressure along the flanks and in the separated region at the rear. If the cylinder is rotating, a net pressure gradient (lift) arises that is transverse to the mean flow direction; this is called the Magnus effect (Prandtl and Tietjens 1934a). Byers (1942) and later Fujita & Grandoso (1968) proposed that cyclonically rotating storms deviate to the right of the mean winds as a result of the horizontal pressure gradients produced by this effect.

A more detailed examination of the flow in and around storms reveals significant complications in the obstacle-flow analogy. Updrafts are entraining and/or detraining substantial amounts of air over most of their vertical height. As the updraft is embedded within a strongly sheared flow, both the magnitude and direction of the storm-relative flow may vary significantly with height. In fact, at the lower levels, the storm-relative flow direction is reversed (see the low-level environmental flow in Figures 2*b* and 9), which would cause the Magnus effect to work in the wrong direction.

In numerical storm simulations, Rotunno & Klemp (1982) found that the pressure gradient across the updraft aligns more consistently with the direction of the shear vector at each level as suggested by linear theory [see Equation (16)] than with the direction of the storm-relative flow. Finally, the updraft is not a tangible entity that can be deflected laterally. Since the updraft is continually regenerated from below, horizontal forces acting on the rising air parcels do not necessarily promote updraft propagation.

Variations on the obstacle-flow analogy were proposed by Newton & Newton (1959) and Alberty (1969). They argued that low pressure on the flanks (Alberty) and downwind (Newton & Newton) of the storm, produced by obstacle-flow effects, cause vertical pressure gradients that induce lifting on the flanks and, thereby, transverse propagation. I believe this approach correctly focuses attention on the influence of verti-

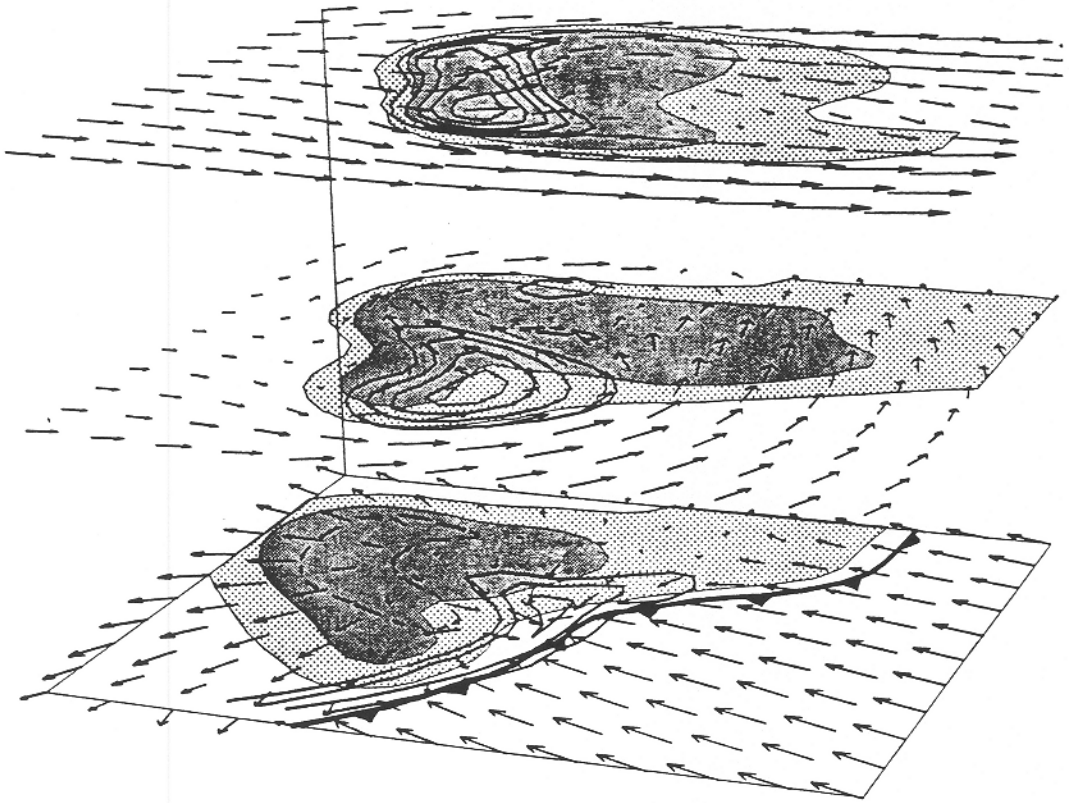

Figure 9 Perspective view of the flow structure within the numerically simulated supercell thunderstorm shown in Figure 8, displayed along horizontal cross sections located at 0, 4, and 8 km above the ground. The horizontal flow vectors are spaced 2 km apart (every second grid point) and are scaled such that the distance separating adjacent vectors corresponds to 25 m s^{-1}. Vertical velocity is contoured in 5 m s^{-1} intervals with the zero line removed except at the lowest level, where w is contoured at z=0.25 km in 1 m s^{-1} increments. Regions of precipitation exceeding 0.5 and 2 g kg^{-1} are differentially shaded, and the barbed line denotes the location of the cold-air boundary at the surface.

cal pressure gradients on propagation, although the inference of pressure distributions from obstacle-flow analogies suffers from the complications mentioned above.

Rotationally Induced Propagation

Based on analyses of numerically simulated supercell storms, Rotunno & Klemp (1985) proposed that storm propagation transverse to the environmental wind shear is dynamically induced by the strong midlevel rotation that develops along the flank of the storm. This mechanism is basically the same as the one responsible for storm splitting (described in Section 3); the strong midlevel rotation on the updraft flank lowers the pressure locally, which promotes lifting pressure gradients and thus new updraft growth that displaces the updraft laterally.

The factors influencing propagation were evaluated by examining again the forcing terms in the vertical momentum equation (6). Rotunno & Klemp found the dynamically induced vertical pressure gradient to be the only term in (6) that causes new growth on the flank of the updraft that is transverse to the wind shear. Although the buoyancy forcing within the updraft is substantial, it is nearly coincident with the updraft and therefore does not contribute to propagation. The nature of the dynamics forcing can be further clarified by considering the terms in (9) that govern the dynamics pressure π_{dn}. By defining $\pi_{dn} = \pi_s + \pi_e$, they computed the contribution to π_{dn} from the fluid shear terms (π_s) and the fluid extension terms (π_e) and established that the shear terms were responsible for the propagation. The fluid extension terms have their strongest influence, as expected, along the centerline of the updraft.

To further isolate the dynamically forced pressure gradients, Rotunno & Klemp (1985) recomputed the storm simulation shown in Figures 8 and 9 but now prohibited the formation of precipitating water drops. This was accomplished by allowing water vapor to condense and release latent heat, but not allowing liquid water to fall relative to the air. With the physics altered in this manner, the initial storm still splits and evolves into a mirror-image pair of storms that exhibit strong rotation at midlevels and propagate apart, transverse to the mean wind shear. The downdrafts are much weaker, and no cold outflow occurs beneath the storm (essentially eliminating the downdraft branch of the circulation depicted in Figure 2*b*). Thus, even without the precipitation-driven downdrafts, the forces promoting transverse propagation continue to operate.

The relationship between the updraft and the shear-induced low pressure is depicted in a three-dimensional perspective (viewed from the east) in Figure 10. The low-π_s region corresponds closely in location and amplitude to the full perturbation pressure π; it induces new lifting on the southern flank of the updraft and thereby propagation of the entire storm toward the south. Recalling the qualitative relationship $\nabla^2 \pi_s \sim -\pi_s$, one would expect low pressure to arise where the fluid shear terms are negative

[see Equation (9)]. For a fluid in pure rotation these terms are negative, whereas for a purely shearing flow they are positive or zero (see Prandtl & Tietjens 1934b, p. 82). Thus, Rotunno and Klemp (1985) attributed the lowered pressure to the rotational component of the flow structure.

This study suggests that the gust front may be less important in governing supercell storm propagation than previously believed. Beneath the storm, strong lifting is usually maintained by the convergence of the cold-downdraft outflow and the warm moist inflow (clearly visible in the low-level cross section in Figure 9). Weaver & Nelson (1982) and others have documented that new convection forming along this gust-front-induced convergence line frequently governs storm propagation. However, in this simulation without precipitation (and thus without a low-level gust front), transverse propagation occurs in a similar fashion to that in the full simulation. This result indicates that the cold downdraft outflow may play a secondary role in supercell storm propagation.

In a related study, Weisman & Klemp (1984) computed the contributions of the dynamics and buoyancy forcing terms in (6) to the overall strength of the updraft for both supercellular and nonsupercellular storms. By integrating these terms along updraft trajectories, they found that the dynamics forcing contributed about 60% of the updraft intensity in the supercell storm but only about 35% of the updraft intensity in the non-

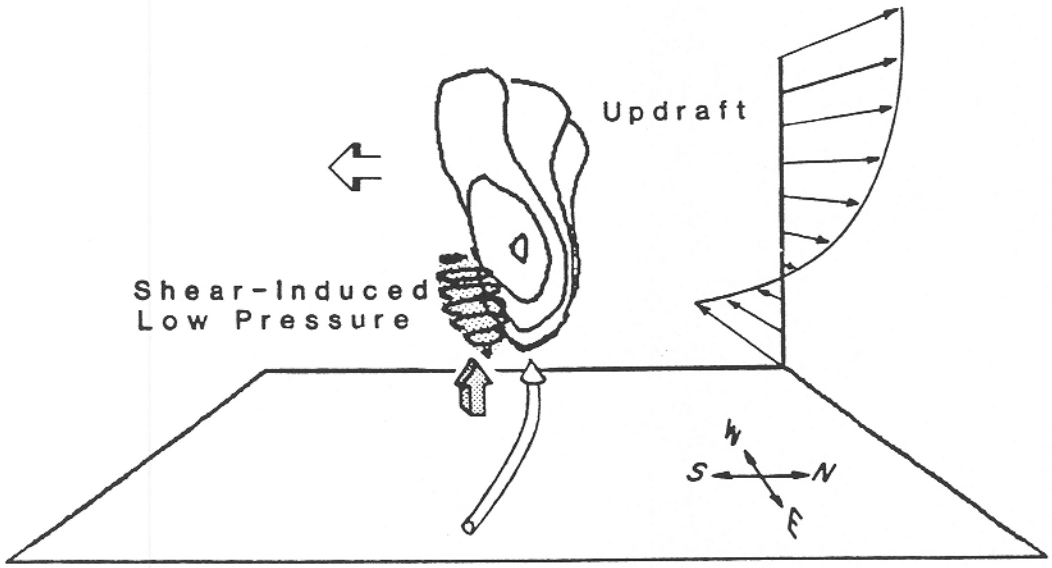

Figure 10 Three-dimensional perspective (looking west) of the updraft (> 20 m s^{-1}) together with the shear-induced pressure (< -3.6 mbar) for a simulation with no precipitation in an environment with unidirectional (westerly) wind shear. The cylindrical arrow indicates the direction of storm-relative inflow, the shaded arrow denotes the rotationally induced forcing, and the open arrow shows the southerly direction of propagation. The displayed surface plane is 20×20 km, and the vertical scale is exaggerated by a factor of two. (Adapted from Rotunno & Klemp 1985.)

supercellular storm. These results suggest that the dynamically induced vertical pressure gradients are fundamentally important in driving a supercell's updraft circulation, as well as in displacing it laterally.

Forced Propagating Gravity Waves

Although the updrafts within convective storms may be highly unstable, they generate substantial perturbations in the surrounding stable environment. An approach developed by Lindzen (1974) and Raymond (1975, 1976) proposes that the motion of convective storms is controlled by propagating gravity waves, forced by the moist convection. The convective heating is parameterized, typically by relating it to the lifting at the level of cloud base caused by the gravity-wave motion. The gravity waves and convection can thus interact symbiotically to generate instabilities that select the preferred modes — termed *wave-CISK* by Lindzen (1974). This mechanism is a variation on CISK (Conditional Instability of the Second Kind), which was introduced by Charney & Eliassen (1964) and Ooyama (1964) to explain the role of small-scale convection in intensifying hurricanes.

In applying wave-CISK, one solves the linear wave equations subject to an appropriate forcing term that represents the nonlinear aspects of the system, most particularly the moist convection. To illustrate this approach, we consider the linear inviscid equations, ignoring vertical variations in the mean density. The thermodynamic equation, expressed in terms of the buoyancy B, can be written as

$$\frac{\partial B}{\partial t} + \boldsymbol{V} \cdot \nabla_h B + N^2 w = Q, \tag{18}$$

where N is the buoyancy frequency (also called the Brunt-Väisälä frequency), and Q is the latent heating term, which can be approximated by the vertical mass flux through cloud base at $z = b$ multiplied by the average gradient of nonadiabatic heating between cloud base and cloud top (see Raymond 1975, Lilly 1979):

$$Q = \begin{cases} N^2 b \frac{\partial w}{\partial z}|_{z=0}, & \text{if } \frac{\partial w}{\partial z}|_{z=0} > 0; \\ 0, & \text{otherwise.} \end{cases} \tag{19}$$

Combining (18) with the linearizations of (1) and (2) and considering disturbances of the form $w = \hat{w}(z) exp[i(\boldsymbol{k} \cdot \boldsymbol{x} - ct)]$ yields the Taylor–Goldstein equation (*cf.* Drazin & Reid 1981) with a forcing term:

$$\frac{\partial^2 \hat{w}}{\partial z^2} + \left\{ \frac{N^2}{(c - V_k)^2} + \frac{1}{(c - V_k)} \frac{d^2 V_k}{dz^2} - k^2 \right\} \hat{w} = \frac{\epsilon \hat{Q}}{(c - V_k)^2}, \tag{20}$$

where $\boldsymbol{k}$ is the horizontal vector wave number, c is the phase speed, $V_k = \boldsymbol{V} \cdot \boldsymbol{k}/k$ is the component of $\boldsymbol{V}$ in the direction of $\boldsymbol{k}$, and $k = |\boldsymbol{k}|$. The

factor ϵ arises in the Fourier modes from the constraint $Q \geq 0$ imposed in (19), and Lindzen (1974) showed that $\epsilon = 1/2$ is an appropriate estimate. Solving for the eigenmodes of (20), one seeks the most unstable mode to characterize the nature of the propagating disturbance.

Raymond (1975, 1976) solved this equation for observed wind profiles associated with several supercell and splitting-storm cases. The resulting estimates for the motion of the most unstable modes were generally in good agreement with the observed storm propagation if he overestimated the heating using a value of $\epsilon = 3/2$. However, to generate splitting and transverse propagating modes, the wave-CISK model required directional turning of the environmental wind-shear vector. This requirement is contrary to the results of three-dimensional numerical cloud models that consistently produce splitting storms (such as that shown in Figures 8 and 9) in strong unidirectional wind shear. Also, the neglect of the nonlinear terms in the momentum equation may be a crucial deficiency when applied to supercell storms developing in strong wind shear.

Raymond (1983) reformulated the wave-CISK equation in terms of a parameterized mass flux and increased the realism of the model by allowing for lagged feedback influences in both updrafts and downdrafts. This model uses the more reasonable value of $\epsilon = 1/2$ and produces good agreement with observations for simulations of midlattitude and tropical squall lines (Raymond 1984). Currently, however, it does not seem that wave-CISK is a viable candidate for explaining supercell propagation.

Optimization of Helicity

Recently, Lilly (1986b) demonstrated that supercell storms have a highly helical circulation and proposed that this helicity promotes the longevity and transverse propagation of these storms. The helicity H is defined as the inner product of vorticity and velocity, $H \equiv \boldsymbol{\omega} \cdot \boldsymbol{v}$. A more useful dimensionless parameter, relative helicity RH, results from normalizing the helicity by $|\boldsymbol{\omega}||\boldsymbol{v}|$ such that RH lies in the range of ± 1. Lilly points to recent research that has established the importance of helicity in stabilizing turbulent flows. Highly helical eddies are found to decay much more slowly than those with low helicity and thus eventually become dominant in the flow. He proposes that high helicity may similarly reduce the turbulent dissipation in supercell storms and thereby enhance their longevity. Consequently, Lilly suggests that as a supercell develops, it should evolve naturally into a structure that optimizes its helicity.

To illustrate the highly helical nature of supercells, Lilly computed RH throughout a numerically simulated storm and showed that below a height of about 10 km, the average value of RH was about 0.5. As an example of purely helical flow, Lilly considered Beltrami flows in which, by definition, the vorticity is everywhere parallel to the velocity, such that $\boldsymbol{\omega} = \kappa \boldsymbol{v}$. Since $-\nabla^2 \boldsymbol{v} = \nabla \times \boldsymbol{\omega} = \kappa \boldsymbol{\omega} = \kappa^2 \boldsymbol{v}$, the proportionality constant κ equals the magnitude of the three-dmensional wave number $|\boldsymbol{k}|$. If both the

mean and perturbation flows are helical, the combined flow is helical only if the Beltrami coefficient for each flow is the same. For a unidirectional (westerly) wind shear, Lilly estimated the transverse propagation speed c_y by inserting κ for the disturbance (storm) into the mean flow Beltrami equation, with the result

$$\kappa^2 = 2\left(\frac{\pi}{W}\right)^2 + \left(\frac{\pi}{h}\right)^2 = \left(\frac{dU/dz}{-c_y}\right)^2, \tag{21}$$

where the half wavelengths h and W correspond to the height and width of the updraft, respectively. Solving for the propagation speed yields

$$c_y = \pm\gamma h dU/dz, \quad where \quad \gamma = (1 + 2h^2/W^2)^{-\frac{1}{2}}\pi^{-1}. \tag{22}$$

Although this expression is derived from highly idealized assumptions and requires a knowledge of the scale of the storm, it seems to provide qualitatively reasonable estimates of the transverse propagation speed. For example, setting $h = W = 10$ km and $dU/dz = .005\ s^{-1}$ (5 m s^{-1} per km), $c_y \simeq 9$ m s^{-1}.

The role of helicity in supercell thunderstorm dynamics is an intriguing issue that will surely be further analyzed in future research. However, the concept of optimizing helicity is difficult to test; it implies that a whole range of structures could exist (each with a different overall helicity) and that the stabilizing influence of helicity selects the optimal state. Since in nature and in numerical simulations we see only the structure that does evolve, it is hard to judge whether or not this structure is optimal. Also, I feel the importance of minimizing dissipation in supercells storms must be studied further. Supercells are continuously forced by both buoyant and dynamical processes, and the residence time of air parcels within such a storm is short compared to the storm's lifetime. Therefore, it is not yet clear if minimizing dissipation is a key factor influencing the behavior of the storm.

6. TRANSITION TO THE TORNADIC PHASE

Although not all supercell storms produce tornadoes, most of the intense tornadoes are generated by them. In a radar study of Oklahoma storms during 1971–1975, for example, Burgess (1976) found that 62% of the 37 storms that exhibited strong storm-scale rotation developed tornadoes while none occurred in storms which did not rotate.

When a storm does move into its tornadic phase, significant alteration of the storm-scale structure occurs that disrupts the nearly steady configuration ilustrated in Figures 2*b* and 9. Lemon & Doswell (1979) provide an excellent description of storm features that are consistently observed during this transition. These features include a rapid increase in low-level rotation, a decrease in updraft intensity, a small-scale downdraft forming

behind the updraft, and a flow at low levels in which cold-outflow and warm-inflow air spiral around the center of circulation. This low-level flow is depicted schematically in Figure 11; as the downdraft (labeled RFD) adjacent to the updraft intensifies, downdraft outflow progresses cyclonically around the center of rotation (marked by the northern encircled T), which is the likely location for tornado formation. As this outflow pushes into the path of the oncoming moist inflow, a new updraft and center of rotation may also develop tornadic intensity (denoted by the southern encircled T in Figure 11). At the same time, the spreading downdraft outflow cuts off the supply of warm moist air to the original circulation center (called *occlusion*), causing the original updraft to weaken.

Although a supercell storm may persist in a nearly steady configuration for up to several hours, the transition to the tornadic phase illustrated

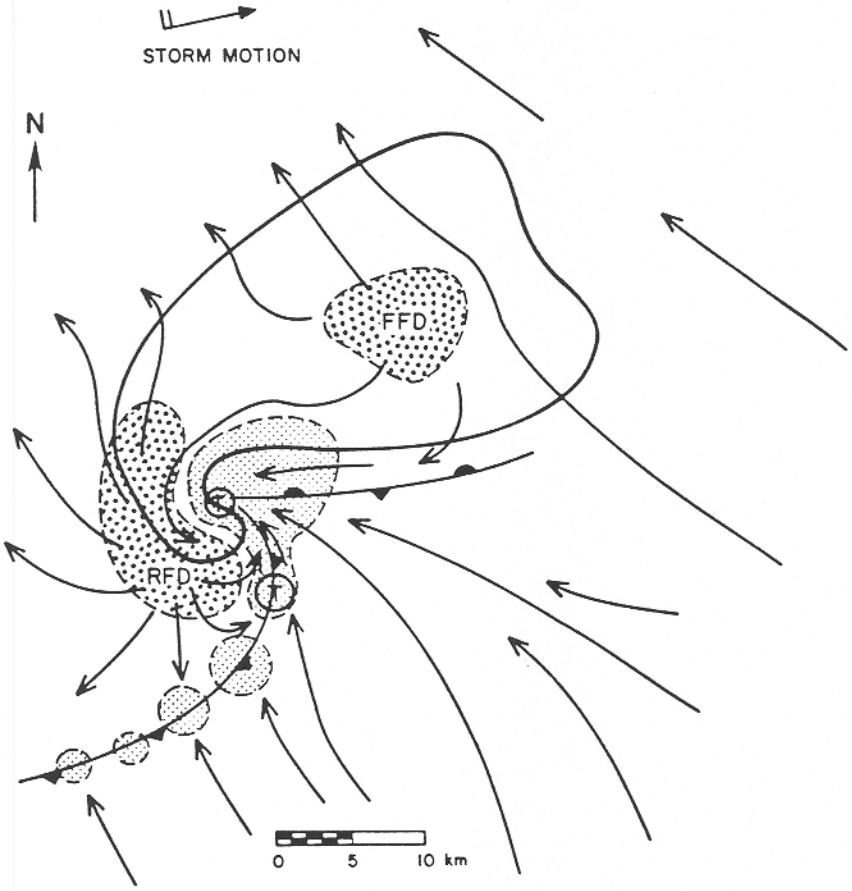

Figure 11 Schematic plan view of a tornadic thunderstorm near the surface. The thick line encompasses the radar echo. The barbed line denotes the boundary between the warm inflow and cold outflow and illustrates the occluding gust front. Low-level position of the updraft is finely stippled, while the forward-flank (FFD) and rear-flank (RFD) downdrafts are coarsely stippled. Storm-relative surface flow is shown along with the likely location of tornadoes (encircled T's). (From Lemon & Doswell 1979, as adapted by Davies-Jones 1985.)

in Figure 11 may take place in less than about 10 min. Barnes (1978) and Lemon & Doswell (1979) have suggested that this transition is initiated by the rear-flank downdraft (see Figure 11), which forms at midlevels, descends to the surface, and then intensifies the low-level rotation by producing strong shear (Barnes) or temperature gradients (Lemon & Doswell) between this downdraft and the updraft.

More recent numerical storm simuations (Klemp & Rotunno 1983, Rotunno & Klemp 1985) and observational studies (Brandes 1984a,b) indicate a reverse sequence of events; the low-level rotation intensifies, followed by formation of the rear flank downdraft. Figure 12 illustrates schematically the flow structure within a numerically simulated supercell evolving in a unidirectional wind shear (as in Figures 8 and 9) at a time when the low-level rotation is intensifying rapidly, but prior to the formation of the occluded gust front shown in Figure 11.

Klemp & Rotunno (1983) proposed that the rear-flank downdraft that promotes this occlusion is, in fact, dynamically induced as strong low-level rotation lowers the pressure locally and draws down air from above. By decomposing the pressure field at a time when the simulated rear-flank

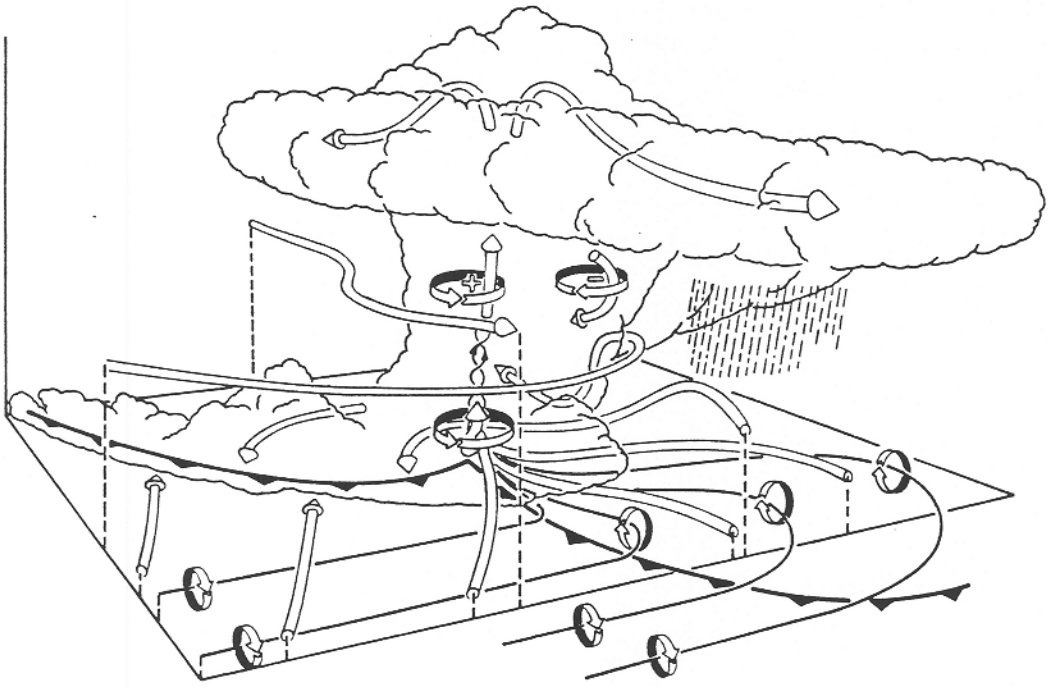

Figure 12 Three-dimensional schematic view of a numerically simulated supercell thunderstorm at a stage when the low-level rotation is intensifying. The storm is evolving in westerly environmental wind shear and is viewed from the southeast. The cylindrical arrows depict the flow in and around the storm. The thin lines show the low-level vortex lines, with the sense of rotation indicated by the circular-ribbon arrows. The heavy barbed line marks the boundary of the cold air beneath the storm.

downdraft was intensifying, they demonstrated that the fluid shear term $\partial v/\partial x \cdot \partial u/\partial y$ was responsible for virtually the entire adverse vertical pressure gradient near the ground. As discussed earlier, a region in pure rotation satisfies $\partial v/\partial x \cdot \partial u/\partial y = -\frac{1}{4}\zeta^2$, and thus qualitatively we have $\pi \sim -\zeta^2$. Since the intensifying ζ is largest near the ground, a downward-directed pressure gradient results, which in turn promotes the downdraft. The retarding influence of rotation has been recognized in a variety of fluid flows (*cf.* Binnie & Hookings 1948) and has been called the *vortex valve* effect; Lemon *et al.* (1975) suggested that as the rotation increases within the storm, this effect may be responsible for its collapse.

An expanded view of the low-level flow in Figure 12 is displayed in Figure 13*a* and indicates the location of the rotation-induced low pressure. As the rear-flank downdraft intensifies, the downdraft outflow spreads out near the ground and, as shown in Figure 13*b*, initiates a new center of convergence and rotation farther east along the gust front (as also depicted in Figure 11). The descending air in the rear-flank downdraft evaporates the cloud water and produces a region of cloud-free air (called the *clear slot*) immediately behind the convergence line, as indicated in Figure 13*b*.

In the numerical simulation just described, the maximum low-level vertical vorticity remained less than one half the maximum at midlevels for over an hour, and then in less than 10 min it intensified to double the midlevel maximum. What factors are responsible for this rapid amplification of the low-level rotation? Analyses of the storm simulations demonstrate clearly that the intensification is stimulated by the baroclinic generation of strong horizontal vorticity [see Equation (4)] along the low-level boundary of the cold air pool forming beneath the storm (Klemp & Rotunno 1983, Rotunno & Klemp 1985). This horizontal vorticity is then tilted into the vertical and strongly stretched as the inflow enters the low-level updraft. To see how this situation arises, notice that in the evolving storm, precipitation is swept around to the northern side of the cyclonically rotating storm. As it falls to the north and northeast of the updraft, evaporation cools the low-level air (see Figure 9). With time, this cold pool of air advances progressively into the path of the low-level inflow to the storm. By the time shown in Figure 9, a significant portion of the inflow is approaching along the boundary of this cold air pool. The horizontal temperature gradients thus baroclinically generate horizontal vorticity that is nearly parallel to the inflowing streamlines. This process generates horizontal vorticity that is several times the magnitude of the mean shear vorticity and that is more favorably oriented to be tilted into vertical cyclonic vorticity. This same mechanism may also be responsible for tornadoes that form occasionally in non-supercellular storms. If a storm encounters a pre-existing cold front or an outflow boundary from another storm, strong horizontal vorticity (baroclinically generated along that boundary) may be swept into the storm and amplified.

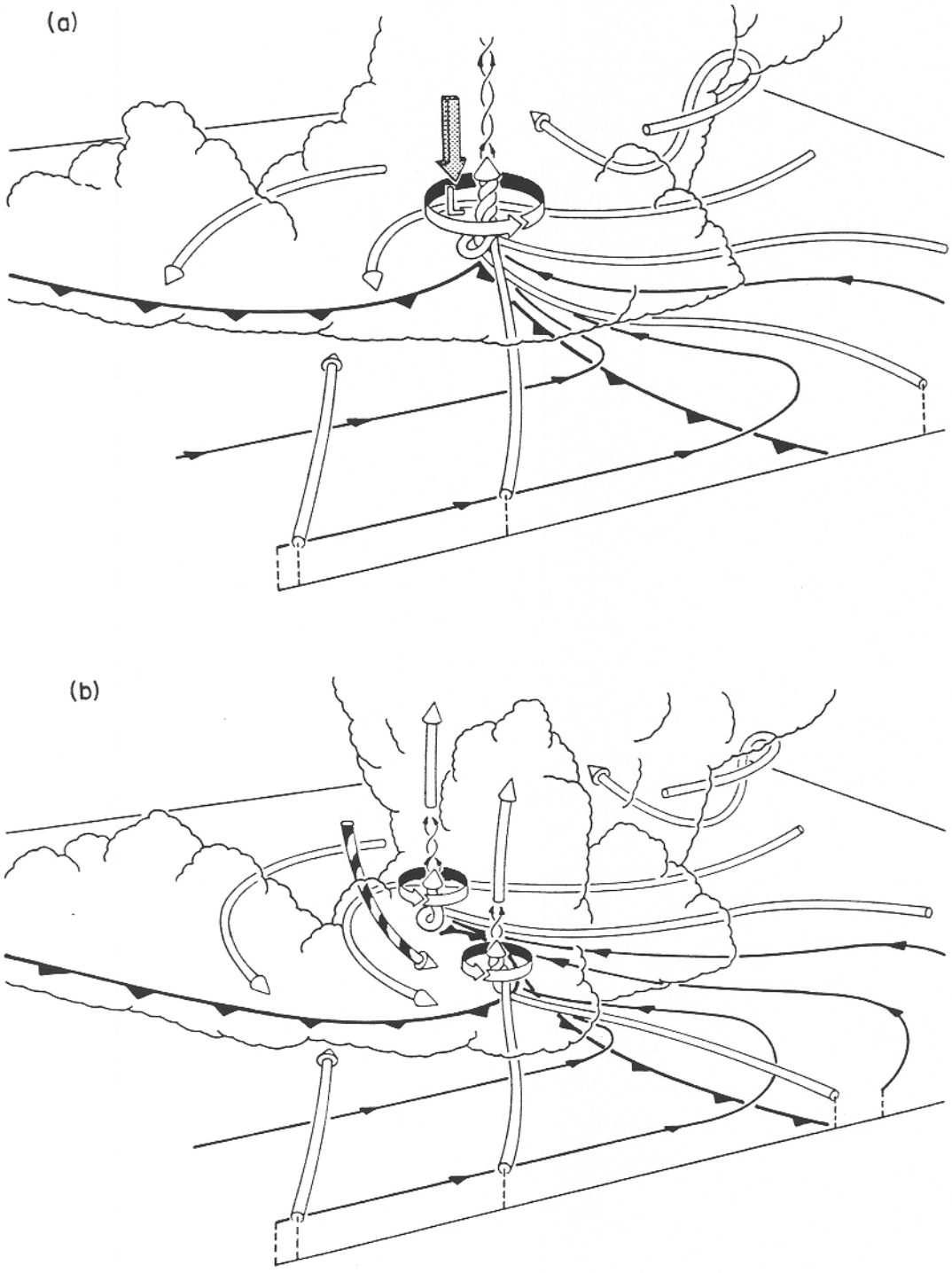

Figure 13 Expanded three-dimensional perspective, viewed from the southeast, of the low-level flow (*a*) at the time depicted in Figure 12, and (*b*) about 10 min later after the rear-flank downdraft has intensified. Features are drawn as described in Figure 12 except that the vector direction of vortex lines are indicated by arrows along the lines. The shaded arrow in (*a*) represents the rotationally induced vertical pressure gradient, and the striped arrow in (*b*) denotes the rear-flank downdraft.

The low-level vortex lines depicted in Figures 12 and 13 further illustrate the baroclinic vorticity generation mechanism. Since the environmental shear is westerly, the horizontal vortex lines embedded in the shear are oriented south–north with the sense of rotation as indicated in the undisturbed region southeast of the storm in Figure 12. As these vortex lines penetrate the low-level pool of cold air, they turn rapidly toward the center of convergence and are swept into the updraft. At this stage, the low-level updraft is located along the boundary between the warm and cold air, and it intertwines the warm and cold flow in the rising air. As the rear-flank downdraft intensifies, this baroclinic generation supports the rapid intensification of rotation in the secondary updraft forming farther to the east along the gust front in Figure 13*b*. After the original updraft is cut off from the warm inflow, it begins to dissipate while the new updraft continues to strengthen. The strong rotation may then cause a new downdraft that spreads out at the surface, cuts off the inflow to this updraft, and promotes yet another convergence center farther east. (In Figure 13, visualize the eastern circulation center in 13*b* becoming the center shown in 13*a*, and then repeating the cycle.) Such redevelopments, accompanied by successive tornadoes, are not uncommon in tornadic storms (Burgess *et al.* 1982).

In recent years new analysis techniques have been devised to calculate the pressure and buoyancy fields from the three-dimensional wind fields derived from multiple-Doppler radar observations (*cf.* Gal-Chen 1978, Hane & Scott 1978). Although the individual schemes vary in their approach, they all compute the pressure and buoyancy fields from the momentum and continuity equations (1)—(2) after estimating all of the kinematic terms from the radar data. These thermodynamic retrieval procedures provide the potential for dramatic advances in convective storm research and for more comprehensive intercomparisons between models and observations. Already, researchers have begun to apply these analysis techniques in studying tornadic storms (Pasken & Lin 1982, Lin & Pasken 1982, Brandes 1984a).

Brandes (1984a) used retrieved thermodynamic data to investigate the transition to the tornadic phase in two storms. He also found that the intensifying low-level rotation was colocated with a region of lowered pressure that promoted the rear-flank downdraft. However, while the derived buoyancy field supported the concept of baroclinic vorticity generation in one storm, it did not in the other. Brandes (1984b) suggested that the stretching of vertical vortex tubes within the low-level updraft may be a more important factor in amplifying the vorticity. This stretching certainly plays an important role in spinning up the vertical vorticity in the baroclinic mechanism as well. A more basic question is, What causes this process to begin to amplify suddenly? I believe the procedures used in retrieving thermodynamic variables are particularly sensitive to the storm

structure near the ground, where there are strong gradients in both the kinematic and thermodynamic fields but often a lack of data from the radar. Further studies will certainly help to clarify these issues.

7. DISCUSSION

The advancements in thunderstorm research have documented clearly that the strong rotation within supercells is a dominant factor in shaping the very special characteristics of these storms. This rotation is derived primarily from horizontal vorticity embeded in the environmental wind shear that is swept up into the storm and tilted toward a vertical axis. The strong rotation on the flanks of the midlevel updraft promotes splitting of the initial convective cell as well as transverse propagation of the storm. This rotation also contributes to the formation of a long-lived structure in which the precipitating downdrafts support, rather than destroy, continued convection. As evaporatively cooled air moves into the path of the storm's inflow, baroclinic generation of horizontal vorticity along the boundary of this cold air causes the intensification of low-level rotation that may trigger the transition of a storm into its tornadic phase.

An important question that remains unresolved is, How is the tornadic circulation embedded within the storm-scale structure? The tornado itself appears nearly axisymmetric, while the storm structure in the vicinity of the tornado (along the boundary between warm-updraft and cold-downdraft air) is highly asymmetric. In both numerical models and observations, the issue is complicated by the nearly two orders of magnitude difference in the horizontal scale of the tornado and the parent storm. Future research with high-resolution radar and more powerful supercomputers will undoubtedly contribute to the resolution of this outstanding issue.

To date, tornadic thunderstorm research has led to a refined understanding of the environmental conditions that promote these storms and an improved ability to identify the salient features within an evolving storm that indicate a strong likelihood of impending tornadic activity. Other factors, however, such as the storm-initiation processes and the interactions between storms and with the larger-scale environment, greatly complicate the prospects for forecasting the precise time and location of tornadoes with a significant lead time. Further research in these areas will be necessary in order to improve this outlook substantially.

Literature Cited

Achtemeier, G. L. 1969. Some observations of splitting thunderstorms over Iowa on August 25–26, 1965. *Preprints, Conf. Severe Local Storms, 6th,* pp. 89–94. Boston: Am. Meteorol. Soc.

Alberty, R. L. 1969. A proposed mechanism for cumulonimbus persistence in the presence of strong vertical shear. *Mon. Weather Rev.* 97:590–96

Barnes, S. L. 1970. Some aspects of a severe right-moving thunderstorm deduced from mesonetwork observations. *J. Atmos. Sci.* 27:634–48

Barnes, S. L. 1978. Oklahoma thunderstorms on 29–30 April 1970. Part I: Morphology of a tornadic storm. *Mon. Weather Rev.* 106:673–84

Binnie, A. M., Hookings, G. A. 1948. Laboratory experiments on whirlpools. *Proc. R. Soc. London Ser. A* 194:348–415

Brandes, E. A. 1977. Gust front evolution and tornado genesis as viewed by Doppler radar. *J. Appl. Meteorol.* 16:333–38

Brandes, E. A. 1978. Mesocyclone evolution and tornadogenesis: some observations. *Mon. Weather Rev.* 106:995–1011

Brandes, E. A. 1984a. Relationships between radar-derived thermodynamic variables and tornadogenesis. *Mon. Weather Rev.* 112:1033–1052

Brandes, E. A. 1984b. Vertical vorticity generation and mesocyclone sustenance in tornadic thunderstorms: the observational evidence. *Mon. Weather Rev.* 112:2253–69

Brooks, E. M. 1949. The tornado cyclone. *Weatherwise* 2:32–33

Browning, K. A. 1964. Airflow and precipitation trajectories within severe local storms which travel to the right of the winds. *J. Atmos. Sci.* 21:634–39

Browning, K. A. 1968. The organization of severe local storms. *Weather.* 23:429–34

Browning, K. A., Donaldson, R. J. Jr. 1963. Airflow structure of a tornadic storm. *J. Atmos. Sci.* 20:533–45

Browning, K. A., Foote, G. B. 1976. Airflow and hailgrowth in supercell storms and some implications for hail suppression. *Q. J. R. Meteorol. Soc.* 102:499–533

Browning, K. A., Landry, C. R. 1963. Airflow within a tornadic storm. *Preprints, Weather Radar Conf., 10th,* pp. 116–22. Boston: Am. Meteorol. Soc.

Browning, K. A., Ludlam, F. H. 1962. Airflow in convective storms. *Q. J. R. Meteorol. Soc.* 88:117–35

Burgess, D. W. 1976. Single Doppler radar vortex recognition. Part 1: mesocyclone signatures. *Preprints Conf. Radar Meteorol., 17th,* pp. 97–103. Boston: Am. Meteorol. Soc.

Burgess, D. W., Wood, V. T., Brown, R. A. 1982. Mesocyclone evolution statistics. *Preprints, Conf. Severe Local Storms, 12th,* pp. 422–24. Boston: Am. Meteorol. Soc.

Byers, H. R. 1942. Nonfrontal thunderstorms. *Misc. Rep. No. 3.* Chicago: Univ. Chicago Press. 26 pp.

Byers, H. R., Braham, R. R. Jr. 1949. *The Thunderstorm.* Washington DC: Govt. Print. Off. 287 pp.

Charba, J., Sasaki, Y. 1971. Structure and movement of the severe thunderstorms of 3 April 1964 as revealed from radar and surface mesonetwork data analysis. *J. Meteorol. Soc. Japan.* 49:191–213

Charney, J. G., Eliassen, A. 1964. On the growth of the hurricane depression. *J. Atmos. Sci.* 21:68–75

Davies-Jones, R. P. 1984. Streamwise vorticity: the origin of updraft rotation in supercell storms. *J. Atmos. Sci.* 41:2991–3006

Davies-Jones, R. P. 1985. Tornado dynamics. See Kessler 1985, pp. 197–236

Drazin, P. G., Reid, W. H. 1981. *Hydrodynamic Stability,* Cambridge: Cambridge Univ. Press. 525 pp.

Dutton, J. A. 1976. *The Ceaseless Wind.* New York: McGraw-Hill. 579 pp.

Eagleman, J. R., Lin, W. C. 1977. Severe thunderstorm internal structure from dual-Doppler radar measurements. *J. Appl. Meteorol.* 16:1036–48

Fankhauser, J. C. 1971. Thunderstorm-environment interactions determined from aircraft and radar observations. *Mon. Weather Rev.* 99:171–192

Fujita, T., Grandoso, H. 1968. Split of a thunderstorm into anticyclonic and cyclonic storms and their motion as determined from numerical model exper-

iments. *J. Atmos. Sci.* 25:416–39

Gal-Chen, T. 1978. A method for the initialization of the anelastic equations: implications for matching models with observations. *Mon. Weather Rev.* 106:587–606

Hammond, G. R. 1967. Study of a left moving thunderstorm of 23 April 1964. *ESSA Tech. Memo.* IERTM-NSSL 31, Natl. Severe Storms Lab., Norman, Okla. 75 pp.

Hane, C. E., Scott, B. C. 1978. Temperature and pressure perturbations within convetive clouds derived from detailed air motion. Preliminary testing. *Mon. Weather Rev.* 106:654–61

Hitschfeld, W. 1960. The motion and erosion of convective storms in severe vertical wind shear. *J. Meteorol.* 17:270–82

Houze, R. A. Jr., Hobbs, P. V. 1982. Organization and structure of precipitating cloud systems. *Adv. Geophys.* 24:225–315

Kessler, E., ed. 1985. *Thunderstorm Morphology and Dynamics.* Norman: Univ. Okla. Press. 411 pp. 2nd ed.

Klemp, J. B., Rotunno, R. 1983. A study of the tornadic region within a supercell thunderstorm. *J. Atmos Sci.* 40:359–77

Klemp, J. B., Weisman, M. L. 1983. The dependence of convective precipitation patterns on vertical wind shear. *Preprints, Conf. Radar Meteorol., 21st,* pp. 44–49. Boston: Am. Meteorol. Soc.

Klemp, J. B., Wilhelmson, R. B. 1978. Simulations of right- and left-moving storms produced through storm splitting. *J. Atmos. Sci.* 35:1097–1110

Klemp, J. B., Wilhelmson, R. B., Ray, P. S. 1981. Observed and numerically simulated structure of a mature supercell thunderstorm. *J. Atmos. Sci.* 38:1558–80

Kropfli, R. A., Miller, L. J. 1976. Kinematic structure and flux quantities in a convective storm from dual-Doppler radar observations. *J. Atmos. Sci.* 33:520–29

Lemon, L. R., Doswell, C. A. III. 1979. Severe thunderstorm evolution and mesocyclone structure as related to tornadogenesis. *Mon. Weather Rev.* 107:1184–97

Lemon, L. R., Burgess, D. W., Brown, R. A. 1975. Tornado production and storm sustenance. *Preprints, Conf. Severe Local Storms, 9th,* pp. 100–4. Boston: Am. Meteorol. Soc.

Lilly, D. K. 1979. The dynamical structure and evolution of thunderstorms and squall lines. *Ann. Rev. Earth and Planet. Sci.* 7:117–61

Lilly, D. K. 1982. The development and maintenance of rotation in convective storms. In *Intense Atmospheric Vortices.*, ed. L. Bengtsson, J. Lighthill, pp. 149–60. Berlin: Springer-Verlag.

Lilly, D. K. 1986a. The structure, energetics and propagation of rotating convective storms. Part I: Energy exchange with the mean flow. *J. Atmos. Sci.* 43:113–25

Lilly, D. K. 1986b. The structure, energetics and propagation of rotating convective storms. Part II: Helicity and storm stabilization. *J. Atmos. Sci.* 43:126–40

Lin, Y. J., Pasken, R. 1982. Thermodynamic structure of a tornadic storm as revealed by dual-Doppler data. *Preprints, Conf. Severe Local Storms, 12th,* pp. 405–8. Boston: Am. Meteorol. Soc.

Lindzen, R. S. 1974. Wave-CISK in the tropics. *J. Atmos. Sci.* 31:156–79

Maddox, R. A. 1976. An evaluation of tornado proximity wind and stability data. *Mon. Weather Rev.* 104:133–42

Miller, L. J. 1975. Internal airflow of a convective storm from dual-Doppler radar measurements. *Pure Appl. Geophys.* 113:765–85

Miller, M. J., Pearce, R. 1974. A three-dimensional primitive equation model of cumulus convection. *Q. J. R. Meteorol. Soc.* 100:133–54

Morton, R. B. 1966. Geophysical vortices. In *Progress in Aeronautical Sciences*, ed. D. Küchmann, 7:145–94. Oxford/London: Pergamon. 220 pp.

Newton, C. W. 1963. Dynamics of severe convective storms. In *Meteorological Monographs*, ed. D. Atlas *et al.*, 5:33–58. Boston: Am. Meteorol. Soc. 247 pp.

Newton, C. W., Fankhauser, J. C. 1964. On the movements of convective storms, with emphasis on size discrimination in relation to water-budget requirements. *J. Appl. Meteorol.* 3:651–68

Newton, C. W., Katz, S. 1958. Movement of large convective rain storms in rela-

tion to winds aloft. *Bull. Am. Meteorol. Soc.* 32:129–36

Newton, C. W., Newton, H. R. 1959. Dynamical interactions between large convective clouds and environment with vertical shear. *J. Meteorol.* 16:483–96

Ogura, Y., Phillips, N. A. 1962. Scale analysis of deep and shallow convection in the atmosphere. *J. Atmos. Sci.* 19:173–79

Ooyama, K. 1964. A dynamical model for the study of tropical cyclone development. *Geofis. Int.* 4:187–98

Pasken, R., Lin, Y. J. 1982. Pressure perturbations within a tornadic storm derived from dual-Doppler wind data. *Preprints, Conf. Severe Local Storms, 12th,* pp 257–60. Boston: Am. Meteorol. Soc.

Prandtl, L., Tietjens, O. G. 1934a. *Applied Hydro- and Aero-mechanics.* New York: Dover. 311 pp. 1957 ed.

Prandtl, L., Tietjens, O. G. 1934b. *Fundamentals of Hydro- and Aero-Mechanics.* New York: Dover. 270 pp. 1957 ed.

Ray, P. S., Doviak, R. J., Walker, G. B., Sirmans, D., Carter, J., Bumgarner, B. 1975. Dual-Doppler observation of a tornadic storm. *J. Appl. Meteorol.* 14:1521–30

Ray, P. S., Johnson, B. C., Johnson, K. W., Bradberry, J. S., Stephens, J. J., *et al.* 1981. The morphology of several tornadic storms on 20 May 1977. *J. Atmos. Sci.* 38:1643–63

Raymond, D. J. 1975. A model for predicting the movement of continuously propagating convective storms. *J. Atmos. Sci.* 32:1308–17

Raymond, D. J. 1976. Wave-CISK and convective mesosystems. *J. Atmos. Sci.* 33:2392–98

Raymond, D. J. 1983. Wave-CISK in mass flux form. *J. Atmos. Sci.* 40:2561–72

Raymond, D. J. 1984. A wave-CISK model of squall lines. *J. Atmos. Sci.* 41:1946–58

Rotunno, R., 1981. On the evolution of thunderstorm rotation. *Mon. Weather Rev.* 109:171–80

Rotunno, R., Klemp, J. B. 1982. The influence of the shear-induced pressure gradient on thunderstorm motion. *Mon. Weather Rev.* 110:136–51

Rotunno, R., Klemp, J. B. 1985. On the rotation and propagation of simulated supercell thunderstorms. *J. Atmos. Sci.* 42:271–92

Schlesinger, R. E. 1975. A three-dimensional numerical model of an isolated deep convective cloud: preliminary results. *J. Atmos. Sci.* 32:934–57

Schlesinger, R. E. 1980. A three-dimensional numerical model of an isolated deep thunderstorm. Part II: Dynamics of updraft splitting and mesovortex couplet evolution. *J. Atmos. Sci.* 37:395–420

Thorpe, A. J., Miller, M. J. 1978. Numerical simulations showing the role of the downdraught in cumulonimbus motion and splitting. *Q. J. R. Meteorol. Soc.* 104:873–93

Weaver, J. F., Nelson, S. P. 1982. Multiscale aspects of thunderstorm gust fronts and their effects on subsequent storm development. *Mon. Weather Rev.* 110:707–18

Weisman, M. L., Klemp, J. B. 1982. The dependence of numerically simulated convective storms on vertical wind shear and buoyancy. *Mon. Weather Rev.* 110:504–20

Weisman, M. L., Klemp, J. B. 1984. The structure and classification of numerically simulated convective storms in directionally varying wind shears. *Mon. Weather Rev.* 112:2479–98

Wilhelmson, R. B. 1974. The life cycle of a thunderstorm in three dimensions. *J. Atmos. Sci.* 31:1629–51

Wilhelmson, R. B., Klemp, J. B. 1978. A three-dimensional numerical simulation of splitting that leads to long-lived storms. *J. Atmos. Sci.* 35:1037–63

Wilhelmson, R. B., Klemp, J. B. 1981. A three-dimensional numerical simulation of splitting severe storms on 3 April 1964. *J. Atmos. Sci.* 38:1581–1600